Analytic continuation by duality estimation of the *S* parameter

S. R. Ignjatović* and L. C. R. Wijewardhana†
Department of Physics, University of Cincinnati, Cincinnati, Ohio 45221

T. Takeuchi‡
Institute for Particle Physics and Astrophysics, Department of Physics, Virginia Tech, Blacksburg, Virginia 24061
(Received 30 July 1999; published 9 February 2000)

We investigate the reliability of the analytic continuation by duality (ACD) technique in estimating the electroweak *S* parameter for technicolor theories. The ACD technique, which is an application of finite energy sum rules, relates the *S* parameter for theories with unknown particle spectra to known OPE coefficients. We identify the sources of error inherent in the technique and evaluate them for several toy models to see if they can be controlled. The evaluation of errors is done analytically and all relevant formulas are provided in appendixes including analytical formulas for approximating the function $1/s$ with a polynomial in s. The use of analytical formulas protects us from introducing additional errors due to numerical integration. We find that it is very difficult to control the errors even when the momentum dependence of the OPE coefficients is known exactly. In realistic cases in which the momentum dependence of the OPE coefficients is only known perturbatively, it is impossible to obtain a reliable estimate.

PACS number(s): 11.55.Hx, 11.55.Fv, 12.15.Lk, 12.60.Nz

I. INTRODUCTION

The standard $SU(2)_L \times U(1)_Y$ gauge theory of electroweak interactions [1] has been very successful in explaining particle phenomenology at currently available accelerator energies. However, the mechanism of electroweak symmetry breaking (i.e., the Higgs sector) is yet to be understood. Though many theories have been proposed as to what this mechanism is, they cannot be tested directly by accelerator experiments for several more years, at least not until the start of physics at the CERN Large Hadron Collider (LHC). In the meantime, the Higgs sector must be probed indirectly by using precision electroweak measurements.

In recent years, precision electroweak measurements have reached the level of accuracy which enables us to discern between various Higgs sector theories from the difference in the size of radiative corrections [2]. In Ref. [3], it is shown that under a small set of assumptions, vacuum polarization (oblique) corrections from the Higgs sector and/or any new physics beyond the standard model (SM) can be expressed in terms of just three parameters called *S*, *T*, and *U*. These parameters are linear combinations of electroweak vacuum polarization functions and are defined in such a way that *S* represents the ''size'' of the Higgs sector, while *T* and *U* quantify the breaking of custodial symmetry [4]. The dependence of various observables on *S*, *T*, and *U* can be calculated using the star formalism of Kennedy and Lynn [5] and fitting the resulting expressions to the experimental data provides limits on the three parameters which can be compared directly with theory.

Unfortunately, calculating the theoretical values of *S*, *T*, and *U* for strongly interacting theories such as technicolor is not an easy task. One popular approach used by many authors [6] has been to use the low energy effective chiral Lagrangian to calculate the size of radiative corrections due to the Goldstone and pseudo Goldstone degrees of freedom.[1] The drawback of this approach is that the contribution of the heavier degrees of freedom cannot be determined and must be included as undeterminable phenomenological coefficients of the order $O(p^4)$ terms in the chiral Lagrangian [7].

Another method, used to calculate the *T* parameter [8], is the Jackiw-Johnson sum rule [9] which expresses the technipion decay constants as an integral involving the technifermion dynamical mass. This sum rule can be calculated in the approximation dubbed ''dynamical perturbation theory'' by Pagels and Stokar [10] and is known to give the correct order of magnitude estimate of the pion decay constant in QCD. Unfortunately, since the *T* parameter is the *difference* of the charged and neutral technipion decay constants, the reliability of the estimate for *T* using this method is highly suspect. Since we shall be concerned mainly with the *S* parameter in this paper, we will not dwell on this problem any further.

In Ref. [3], the *S* parameter for technicolor was calculated by expressing *S* as a dispersion integral and using rescaled QCD spectral functions in the integrand. The rescaling to different numbers of technicolors, N_{TC}, and technidoublets, N_{D}, was performed using large-*N* arguments [11] and the result can be summarized as

$$S \approx 0.1 N_{\mathrm{D}} N_{\mathrm{TC}}. \tag{1.1}$$

(Note the proportionality of *S* to N_{D} and N_{TC}: thus, the

*Permanent address: Department of Physics, Prirodno-Matematički Fakultet, Mladena Stojanovića 2, 78000 Banja Luka, Republika Srpska, Bosnia and Hercegovina.
†Electronic address: rohana@physics.uc.edu
‡Electronic address: takeuchi@vt.edu

[1]Of the references cited in [6], Johnson, Young, and McKay also include the effect of techni-vector mesons coupled via vector meson dominance.

''size'' of the Higgs sector.) However, this estimate of S is reliable only if the technicolor theory is dynamically similar to QCD. This condition does not hold in more realistic technicolor theories where one has very little idea as to what the spectral functions should look like.[2]

The analytic continuation by duality[3] (ACD) technique developed in Ref. [12] has been suggested in Ref. [13] as a way of computing the S parameter in theories that differ from QCD. The ACD technique consists of using the analyticity of the vacuum polarization functions to convert the dispersion integral for S, which is an integral along the real s axis, into an integral around a large circle in the complex s plane. The value of the integrand is then estimated by *analytically continuing* the operator product expansion (OPE) [14] from the deep Euclidean region. In Ref. [13], the application of the ACD technique to QCD-like technicolor reproduced Eq. (1.1), while for walking technicolor theories [15] it suggested the possibility that S could be negative.

However, other estimations of S for walking technicolor, such as that of Ref. [16] which used the Bethe-Salpeter equation approach, suggest that S is positive even for walking technicolor theories. Furthermore, the mathematical foundations of the ACD technique have been questioned in Ref. [17].

In this paper, we investigate the reliability of the ACD estimate of S. Our plan is as follows: In Sec. II, we first review the definition of the S parameter. In Secs. III and IV, we review the two methods used in the literature to estimate S, namely, the dispersion relation approach and the ACD technique. In Sec. V, we discuss some puzzles pertaining to the ACD estimate of S, and in Sec. VI, we identify the sources of error inherent to the ACD technique. Section VII is the main portion of the paper in which we apply the ACD technique to several toy models to see if it can reproduce the exact value of S. Section VIII concludes. A portion of this work has been presented previously in Ref. [18]. In this paper, we extend and improve upon, and also correct an error[4] in, the analysis reported therein.

II. DEFINITION OF S

We denote by Π_{XY} the $g^{\mu\nu}$ part of the vacuum polarization tensor between two currents J^μ_X and J^ν_Y :

$$ig^{\mu\nu}\Pi_{XY}(s)+(q^\mu q^\nu\text{term})=\int d^4x\, e^{iq\cdot x}\langle J^\mu_X(x)J^\nu_Y(0)\rangle,$$

$$s=q^2.$$

The S parameter is defined in Ref. [3] as

$$S=-4\pi[\Pi'_{VV}(0)-\Pi'_{AA}(0)]$$

where the subscripts V and A denote the neutral isospin-1 vector and axial-vector currents, respectively, and the prime denotes a derivative with respect to s. The contribution of a fermion doublet $\Psi=(U,D)$ to J^μ_V and J^μ_A is given by

$$J^\mu_V=\bar{\Psi}\gamma^\mu\frac{\tau_3}{2}\Psi,$$

$$J^\mu_A=\bar{\Psi}\gamma^\mu\gamma_5\frac{\tau_3}{2}\Psi,$$

where τ_3 is the third Pauli matrix. For latter convenience, we define the functions $\mathcal{F}_V(s)$ and $\mathcal{F}_A(s)$ as

$$\Pi_{VV}(s)\equiv s\mathcal{F}_V(s),$$

$$\Pi_{AA}(s)\equiv\Pi_{AA}(0)+s\mathcal{F}_A(s),$$

and the following shorthand notation for the differences between the vector and axial-vector functions:

$$\Pi(s)\equiv\Pi_{VV}(s)-\Pi_{AA}(s),$$

$$\mathcal{F}(s)\equiv\mathcal{F}_V(s)-\mathcal{F}_A(s).$$

Then,

$$S=-4\pi[\mathcal{F}_V(0)-\mathcal{F}_A(0)]=-4\pi\mathcal{F}(0).$$

Note that our notation is slightly different from either Ref. [3] or Ref. [13], so care is necessary when comparing formulas.

For weakly interacting theories, S can be calculated using ordinary perturbation theory. However, for strongly interacting theories such as technicolor, perturbation theory cannot be used and some other non-perturbative technique must be utilized. In the next sections, we will look at two different methods that have been used in the literature to estimate S for technicolor theories.

III. DISPERSION RELATION FOR THE S PARAMETER

In this section, we will discuss how one can calculate S using a dispersion relation.

The function $\mathcal{F}(s)=\mathcal{F}_V(s)-\mathcal{F}_A(s)$ is analytic in the entire complex s plane except for a branch cut along the positive real s axis starting from the lowest particle threshold contributing to $\mathcal{F}(s)$. Therefore,

$$\mathcal{F}(t)=\frac{1}{2\pi i}\oint_C ds\frac{\mathcal{F}(s)}{s-t}$$

$$=\frac{1}{\pi}\int_{s_0}^{R}ds\frac{\mathrm{Im}\,\mathcal{F}(s)}{s-t-i\epsilon}+\frac{1}{2\pi i}\oint_{|s|=R}ds\frac{\mathcal{F}(s)}{s-t},\quad(3.1)$$

where C denotes the integration contour shown in Fig. 1 [19]. We have used the Schwartz principle of reflection,

$$\mathcal{F}(s^*)=\mathcal{F}^*(s),$$

[2]QCD-like technicolor theories suffer from the FCNC (flavor changing neutral current) problem. Theories that were devised to avoid this problem (e.g. walking technicolor) are supposed to have dynamics that are distinct from QCD. Just how distinct they actually are is still unclear.

[3]The ''duality'' here refers to ''quark-hadron duality.''

[4]See Sec. VII C 2 and footnote 8.

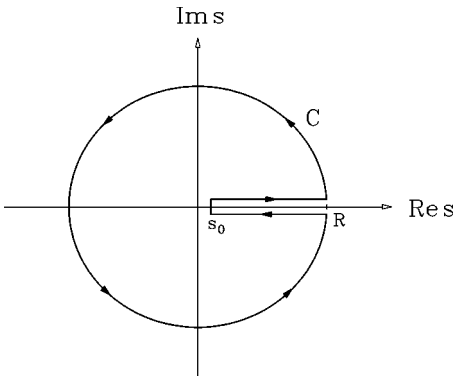

FIG. 1. The contour C which avoids the branch cut along the real s axis.

in expressing the contribution from the part of C which pinches the real axis as an integral involving only the imaginary part of $\mathcal{F}(s)$. In the limit $t\to 0$ we obtain

$$\mathcal{F}(0)=\frac{1}{\pi}\int_{s_0}^{R}\frac{ds}{s}\mathrm{Im}\,\mathcal{F}(s)+\frac{1}{2\pi i}\oint_{|s|=R}\frac{ds}{s}\mathcal{F}(s).$$

It is possible to show that $\mathcal{F}(s)\sim 1/s$ as $s\to\infty$ (using the OPE we will be discussing later) so that the integral around the circle at $|s|=R$ vanishes as $R\to\infty$. Therefore,

$$S=-4\pi\mathcal{F}(0)=-4\int_{s_0}^{\infty}\frac{ds}{s}\mathrm{Im}\,\mathcal{F}(s)$$

$$=-4\int_{s_0}^{\infty}\frac{ds}{s}[\mathrm{Im}\,\mathcal{F}_{\mathrm{V}}(s)-\mathrm{Im}\,\mathcal{F}_{\mathrm{A}}(s)]. \qquad (3.2)$$

Note that in going from the first line to the second, we used only the analyticity of $\mathcal{F}(s)$. No approximation of any sort is involved. Therefore, if the function $\mathrm{Im}\,\mathcal{F}(s)$ were known exactly, we can calculate $\mathcal{F}(0)$ and, hence, the value of S exactly.

Of course, one usually does not know the exact form of the spectral function $\mathrm{Im}\,\mathcal{F}(s)$. In the case of QCD-like technicolor, it can be guessed from the QCD spectral functions with the help of the Weinberg sum rules [20]

$$\frac{1}{\pi}\int_0^{\infty}ds\;\mathrm{Im}\,\mathcal{F}_{\mathrm{TC}}(s)=-f_{\mathrm{TC}}^2,$$

$$\int_0^{\infty}ds\;s\;\mathrm{Im}\,\mathcal{F}_{\mathrm{TC}}(s)=0, \qquad (3.3)$$

where $f_{\mathrm{TC}}\approx 250$ GeV is the technipion decay constant.

Another point one must consider when applying the dispersion relation, Eq. (3.2), to technicolor (TC) is that $\mathrm{Im}\,\mathcal{F}_{\mathrm{TC}}(s)\to -1/48\pi$ as $s\to 0$ due to exactly massless techni Goldstone boson states and we encounter an IR divergence. However, since S is supposed to be the contribution of *new* physics, we must subtract from $\mathrm{Im}\,\mathcal{F}_{\mathrm{TC}}(s)$ the contribution of the SM Higgs sector that technicolor replaces. The exact Goldstone contribution is common to TC theories and the SM, so the IR divergence cancels exactly. Therefore, in the case of technicolor theories, we must calculate

$$S_{\mathrm{TC}}=-4\int_{s_0}^{\infty}\frac{ds}{s}[\mathrm{Im}\,\mathcal{F}_{\mathrm{TC}}(s)-\mathrm{Im}\,\mathcal{F}_{\mathrm{SM}}(s)], \qquad (3.4)$$

where

$$\mathrm{Im}\,\mathcal{F}_{\mathrm{SM}}(s)=-\frac{1}{48\pi}\left[1-\left(1-\frac{m_H^2}{s}\right)^3\theta(s-m_H^2)\right].$$

The lower limit of integration s_0 must be chosen to be below the point where the two spectral functions $\mathrm{Im}\,\mathcal{F}_{\mathrm{TC}}(s)$ and $\mathrm{Im}\,\mathcal{F}_{\mathrm{SM}}(s)$ start to deviate from each other.

In Ref. [3], Eq. (3.4) was used to estimate the value of S_{TC}. First, $\mathrm{Im}\,\mathcal{F}_{\mathrm{V}}(s)$ for QCD was extracted from the $I=1$ part of the $\sigma(e^+e^-\to\text{hadrons})$ data, while $\mathrm{Im}\,\mathcal{F}_{\mathrm{A}}(s)$ for QCD was extracted from the $C=1$ part of the $\Gamma(\tau^-\to\nu_\tau+\text{hadrons})$ data. The Weinberg sum rules, Eqs. (3.3), were used to fix $\mathrm{Im}\,\mathcal{F}_{\mathrm{A}}(s)$ above $s=m_\tau^2$ where data are unavailable. These functions were then parametrized as superpositions of Breit-Wigner resonances,[5] whose masses and widths were rescaled according to the leading large-N approximation [11] to obtain their technicolor counterparts. The resulting form of $\mathrm{Im}\,\mathcal{F}_{\mathrm{TC}}(s)$ was substituted into Eq. (3.4), from which one obtained

$$S\approx 0.1N_{\mathrm{D}}N_{\mathrm{TC}}. \qquad (3.5)$$

IV. ACD TECHNIQUE

In the previous section, the analyticity of $\mathcal{F}(s)$ was exploited to express $\mathcal{F}(0)$ as a contour integral, Eq. (3.1), and the radius of the contour was taken to infinity to make the contribution of the circle around $|s|=R$ vanish. The result was an integral expression for S which only involved the imaginary part of $\mathcal{F}(s)$ along the real positive s axis, i.e. the dispersion relation, Eq. (3.2).

The ACD technique also exploits Eq. (3.1), but instead of making the integral around $|s|=R$ vanish, the integral along the real s axis is made to vanish as follows: Let

$$p_N(s)=\sum_{n=0}^{N}a_n(N)s^n$$

denote polynomials of order N in s where the coefficients $a_n(N)$ are chosen so that as $N\to\infty$ the polynomial $p_N(s)$ converges uniformly onto $1/s$ in the interval $[s_0,R]$; i.e. for any $\epsilon>0$, there exists an integer N_ϵ such that if $N>N_\epsilon$, then

$$\left|\frac{1}{s}-p_N(s)\right|<\epsilon,\quad \forall s\in[s_0,R].$$

Since the product $p_N(s)\mathcal{F}(s)$ is regular inside the contour C shown in Fig. 1, we find

[5]The Gounaris-Sakurai form [21] was used for the ρ.

$$0=\frac{1}{2\pi i}\oint_C ds\, p_N(s)\mathcal{F}(s)$$
$$=\frac{1}{\pi}\int_{s_0}^{R} ds\, p_N(s)\mathrm{Im}\,\mathcal{F}(s)+\frac{1}{2\pi i}\oint_{|s|=R} ds\, p_N(s)\mathcal{F}(s). \tag{4.1}$$

Subtracting Eq. (4.1) from Eq. (3.1), we obtain

$$\mathcal{F}(0)=\frac{1}{\pi}\int_{s_0}^{R} ds\left[\frac{1}{s}-p_N(s)\right]\mathrm{Im}\,\mathcal{F}(s)$$
$$+\frac{1}{2\pi i}\oint_{|s|=R} ds\left[\frac{1}{s}-p_N(s)\right]\mathcal{F}(s). \tag{4.2}$$

If $N>N_\epsilon$, then the absolute value of the first term can be bounded from above by

$$\left|\int_{s_0}^{R} ds\left[\frac{1}{s}-p_N(s)\right]\mathrm{Im}\,\mathcal{F}(s)\right|<\int_{s_0}^{R} ds\left|\frac{1}{s}-p_N(s)\right||\mathrm{Im}\,\mathcal{F}(s)|$$
$$<(R-s_0)\epsilon\mathcal{M},$$

where

$$\mathcal{M}=\max_{s\in[s_0,R]}|\mathrm{Im}\,\mathcal{F}(s)|.$$

Therefore, for sufficiently large N, the integral along the real s axis can be neglected in Eq. (4.2) and we obtain

$$\mathcal{F}(0)\approx\frac{1}{2\pi i}\oint_{|s|=R} ds\left[\frac{1}{s}-p_N(s)\right]\mathcal{F}(s). \tag{4.3}$$

In the deep Euclidean region $-s=Q^2\gg 0$, the value of $\mathcal{F}(s)$ can be expressed in terms of a large momentum expansion

$$\mathcal{F}(s)=\sum_{m=1}^{\infty}\frac{\hat{h}_m}{s^m},\quad s=-Q^2, \tag{4.4}$$

where the coefficients $\hat{h}_m$ can be gleaned from the OPE of $\mathcal{F}(s)$. *Assuming* that Eq. (4.4) is valid all around the circle $|s|=R$ in the complex s plane, then substitution of Eq. (4.4) into Eq. (4.3) gives

$$\mathcal{F}(0)\approx\frac{1}{2\pi i}\oint_{|s|=R} ds\left[\frac{1}{s}-\sum_{n=0}^{N} a_n(N)s^n\right]\sum_{m=1}^{\infty}\frac{\hat{h}_m}{s^m}$$
$$=-\sum_{n=0}^{N}\hat{h}_{n+1}a_n(N).$$

Therefore,

$$S=-4\pi\mathcal{F}(0)\approx 4\pi\sum_{n=0}^{N}\hat{h}_{n+1}a_n(N)\equiv S_{\mathrm{ACD}}. \tag{4.5}$$

This is the ACD technique employed in Ref. [13].

V. PECULIARITIES OF THE ACD TECHNIQUE

The ACD technique introduced in the previous section is peculiar in several respects.

(1) The relation, Eq. (4.5), is *not* an expansion in any small parameter (as far as we can tell), so it is unclear whether the ACD estimate S_{ACD} will converge to the correct value in any limit.

(2) The coefficients of the polynomial $a_n(N)$ which relate the OPE coefficients $\hat{h}_m$ to S_{ACD} depend on the order of the polynomial N, the choice of fit interval $[s_0,R]$, and the fit routine used to fix them, all of which are arbitrary and not dictated by any *physics*. It is therefore difficult to understand what the physics is, if any, behind a relation like Eq. (4.5).

(3) Because of the N dependence of the coefficients $a_n(N)$, the dependence of S_{ACD} on the OPE coefficients $\hat{h}_m$ will change as N is increased. In fact, in the limit that N goes to infinity, the coefficients $a_n(N)$ diverge:

$$\lim_{N\to\infty} a_n(N)=(-1)^n\infty. \tag{5.1}$$

This is due to the simple fact that $1/s$ cannot be Taylor expanded around $s=0$. This means that as N is increased, S_{ACD} will become sensitive to infinitesimal variations in the OPE coefficients $\hat{h}_m$. Since the OPE coefficients $\hat{h}_m$ are only known as products of perturbatively calculable prefactors and uncalculable vacuum expectation values of operators, any uncertainty in them may be considerably enhanced in S_{ACD}.

(4) For QCD/technicolor, the upper limit of the fit interval R must be chosen to be well above the confinement scale Λ_c so that the OPE is applicable at that scale. Then the fit polynomial will be such that $|a_n(N)\Lambda_c^{n+1}|$ decreases monotonically as n is increased for fixed N. Since $\hat{h}_m\sim\Lambda_c^m$, this means that the OPE coefficient $\hat{h}_m$ for larger m will have a smaller contribution to S_{ACD}. However, since $a_n(N)$ is the coefficient of s^n, better and better accuracy is required for the $a_n(N)$'s with larger n for the fit to $1/s$ to be accurate near the end point $s=R$. This is a peculiar situation since the terms that contribute less require better precision.

(5) Whether S is IR divergent or not should be encoded in the OPE coefficients $\hat{h}_m$. However, because the lower limit of the fit interval s_0 cannot be taken to zero, S_{ACD} is always finite and totally blind to any information pertaining to IR divergences. This is in contrast to the dispersion relation approach in which the IR divergence was evident in the spectral function and the SM subtraction was crucial in getting a finite result.

As a result of these peculiarities, the reliability of the relation, Eq. (4.5), is far from clear.

VI. ERRORS INHERENT IN THE ACD TECHNIQUE

In this section, we will take a critical look at the ACD technique and identify where possible errors will be introduced. This will clarify the problems facing the ACD technique and facilitate the discussion of error in the latter sections.

ACD starts from the relation

$$S = S_N + \delta S_{\rm fit}(N)$$

where

$$S_N \equiv -\frac{2}{i}\oint_{|s|=R} ds \left[\frac{1}{s} - p_N(s)\right] \mathcal{F}(s),$$

$$\delta S_{\rm fit}(N) \equiv -4\int_{s_0}^{R} ds \left[\frac{1}{s} - p_N(s)\right] {\rm Im}\, \mathcal{F}(s).$$

For large enough N, the $\delta S_{\rm fit}$ term can be neglected and we can approximate S by S_N:

$$S \approx S_N .$$

We will call the neglected term $\delta S_{\rm fit}(N)$ the *fit error*. It will depend not only on N, but also on the choice of interval $[s_0, R]$, and the fit routine.

In the next step, we assume that the large momentum expansion of $\mathcal{F}(s)$ is known up to M terms:

$$\mathcal{F}(s) = \sum_{n=1}^{M} \frac{h_n(s)}{s^n} + O\left(\frac{1}{s^{M+1}}\right).$$

In general, the coefficients $h_n(s)$ will depend on s. This expansion also may not be a convergent series but just an asymptotic one [22]. Also, such an expansion may not exist all around the circle at $|s|=R$, or it may not exist at all depending on $\mathcal{F}(s)$. But for the moment, let us assume that such an expansion exists. Substituting this expansion in the expression for S_N, we obtain

$$S_N = S_{N,M} + \delta S_{\rm trunc}(N,M)$$

where

$$S_{N,M} = -\frac{2}{i}\oint_{|s|=R} ds \left[\frac{1}{s} - p_N(s)\right] \sum_{n=1}^{M} \frac{h_n(s)}{s^n}$$

$$\delta S_{\rm trunc}(N,M) = -\frac{2}{i}\oint_{|s|=R} ds \left[\frac{1}{s} - p_N(s)\right] \left[\mathcal{F}(s) - \sum_{n=1}^{M} \frac{h_n(s)}{s^n}\right].$$

Note that M must be larger than N in order to suppress the neglected terms by inverse powers of R. We call the error introduced by neglecting $\delta S_{\rm trunc}(N,M)$, i.e. the $O(1/s^{M+1})$ term, the *truncation error*. It will depend on N and M and the radius of the contour R.

Finally, we neglect the s dependence of the coefficients $h_m(s)$ and replace them with their values at $s=-R$ where they are known from the OPE:

$$h_m(s) \approx h_m(-R) \equiv \hat{h}_m .$$

This is a rather dangerous approximation to make since the analytic structure of $\mathcal{F}(s)$ will be completely altered. In fact, under this approximation, ${\rm Im}\,\mathcal{F}(s)$ will only consist of derivatives of the delta function at the origin. We define

$$S_{N,M} = S_{\rm ACD} + \delta S_{\rm AC}(N,M),$$

where

$$S_{\rm ACD} = -\frac{2}{i}\oint_{|s|=R} ds \left[\frac{1}{s} - p_N(s)\right] \sum_{n=1}^{M} \frac{\hat{h}_n}{s^n},$$

$$\delta S_{\rm AC}(N,M) = -\frac{2}{i}\oint_{|s|=R} ds \left[\frac{1}{s} - p_N(s)\right] \sum_{n=1}^{M} \frac{h_n(s) - \hat{h}_n}{s^n}.$$

Reference [13] argues that $\delta S_{\rm AC}(N,M)$ can be expected to be highly suppressed and thus negligible since the difference $1/s - p_N(s)$ is approximately zero in the vicinity of the positive real s axis where the difference $h_n(s) - \hat{h}_n$ can be expected to be the largest. The expression for $S_{\rm ACD}$ can be simplified to

$$S_{\rm ACD} = 4\pi \sum_{n=0}^{\min(N,M-1)} \hat{h}_{n+1} a_n(N),$$

since we only pick up the residues of the single poles. We call the neglected term $\delta S_{\rm AC}(N,M)$ when approximating $S_{N,M}$ with $S_{\rm ACD}$ the *analytic continuation error*.

Therefore, in contrast to the dispersion relation approach, the ACD technique relies on a series of approximations. To summarize, the relation between the exact value of S and the ACD estimate $S_{\rm ACD}$ can be written as follows:

$$S = S_N + \delta S_{\rm fit}(N) = S_{N,M} + \delta S_{\rm trunc}(N,M) + \delta S_{\rm fit}(N)$$
$$= S_{\rm ACD} + \delta S_{\rm AC}(N,M) + \delta S_{\rm trunc}(N,M) + \delta S_{\rm fit}(N).$$

The three different sources of error are:

(1) The fit error $\delta S_{\rm fit}(N)$: the error that comes from neglecting the contribution of the integral along the real s axis. It goes to zero in the limit $N \to \infty$.

(2) The truncation error $\delta S_{\rm trunc}(N,M)$: the error that comes from truncating the large momentum expansion of $\mathcal{F}(s)$. If the series is convergent, then it goes to zero as $M \to \infty$.

(3) The analytic continuation error $\delta S_{\rm AC}(N,M)$: the error that comes from neglecting the momentum dependence of the coefficients in the large momentum expansion. It is not clear if it goes to zero in any limit.

In practice, one does not know the numerical values of the $\hat{h}_m$'s exactly either since they are products of perturbatively calculable prefactors and uncalculable vacuum expectation values of operators, the latter of which can only be estimated to an order of magnitude. This presents another source of potentially dangerous error as we discussed in Sec. V. However, our limited knowledge of the $\hat{h}_m$'s necessary for the ACD technique is analogous to our limited knowledge of the spectral function necessary for the dispersion relation approach and can be considered an independent problem from

whether the ACD technique is reliable or not. In other words, we know that the dispersion relation gives the exact value of S *if* the spectral functions are known exactly. So the question that we shall address here is, will the ACD technique give a reliable estimate for S *if* the $\hat{h}_m$'s were known exactly?

We will therefore follow the following strategy to establish (or refute) the reliability of the ACD technique: First, we will introduce several toy model functions for $\mathcal{F}(s)$ such that the imaginary part along the real s axis $\mathrm{Im}\,\mathcal{F}(s)$, the large momentum expansion coefficients $\hat{h}_n$, and the corresponding value of S are known exactly. Then, we will apply both the dispersion relation and ACD techniques to these model functions and (1) check that the dispersion relation approach reproduces the exact result, and (2) calculate the three types of error discussed above for the ACD technique to see if they are under control. By investigating how the behavior of the errors depends on the characteristics of the toy model functions, we should be able to clarify the strengths and limitations of the ACD technique.

VII. COMPARISON OF DISPERSION RELATION AND ACD APPROACHES FOR MODEL SPECTRA

A. Perturbative 1-loop function

Let us first consider the perturbative 1-loop contribution to $\mathcal{F}(s)$ from a fermion doublet of degenerate mass. In this case, it is straightforward to calculate $\Pi_{\mathrm{VV}}(s)$ and $\Pi_{\mathrm{AA}}(s)$. Using dimensional regularization, they are given by

$$\Pi_{\mathrm{VV}}(s)=\frac{1}{4\pi^2}\int_0^1 dx\{x(1-x)s\}\log\left[\frac{m^2-x(1-x)s}{\mu^2}\right],$$

$$\Pi_{\mathrm{AA}}(s)=\frac{1}{4\pi^2}\int_0^1 dx\{x(1-x)s-m^2\}\log\left[\frac{m^2-x(1-x)s}{\mu^2}\right],$$

from which we find

$$\mathcal{F}_{\mathrm{pert}}(s)=\frac{1}{4\pi^2}\frac{m^2}{s}\int_0^1 dx\,\log\left[1-x(1-x)\frac{s}{m^2}\right]=\begin{cases}\dfrac{1}{4\pi^2}\dfrac{m^2}{s}\left[\beta\log\dfrac{\beta+1}{\beta-1}-2\right], & s<0,\\ \dfrac{1}{4\pi^2}\dfrac{m^2}{s}\left[2|\beta|\arctan\dfrac{1}{|\beta|}-2\right], & 0<s<4m^2,\\ \dfrac{1}{4\pi^2}\dfrac{m^2}{s}\left[\beta\left(\log\dfrac{1+\beta}{1-\beta}-i\pi\right)-2\right], & 4m^2<s,\end{cases} \tag{7.1}$$

where

$$\beta=\sqrt{1-\frac{4m^2}{s}}.$$

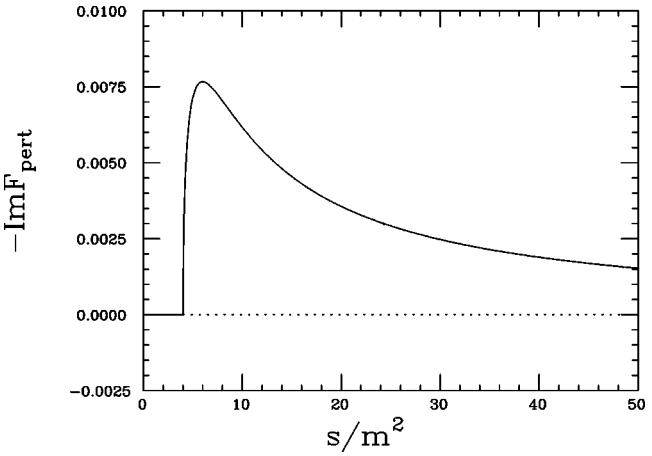

FIG. 2. The perturbative spectral function.

Hence,

$$S_{\mathrm{pert}}=-4\pi\mathcal{F}_{\mathrm{pert}}(0)=\frac{1}{6\pi}. \tag{7.2}$$

1. Dispersion relation: Perturbative spectral function

The imaginary part of the perturbative 1-loop function of Eq. (7.1) is given by

$$\mathrm{Im}\,\mathcal{F}_{\mathrm{pert}}(s)=-\frac{1}{4\pi}\frac{m^2}{s}\beta\,\theta(s-4m^2),\quad \beta=\sqrt{1-\frac{4m^2}{s}}. \tag{7.3}$$

Its plot is shown in Fig. 2. Inserting Eq. (7.3) into Eq. (3.2), we find

$$S_{\mathrm{pert}}=\frac{m^2}{\pi}\int_{4m^2}^{\infty}\frac{ds}{s^2}\sqrt{1-\frac{4m^2}{s}}=\frac{1}{2\pi}\int_0^1\beta^2 d\beta=\frac{1}{6\pi}$$

which recovers Eq. (7.2) exactly.

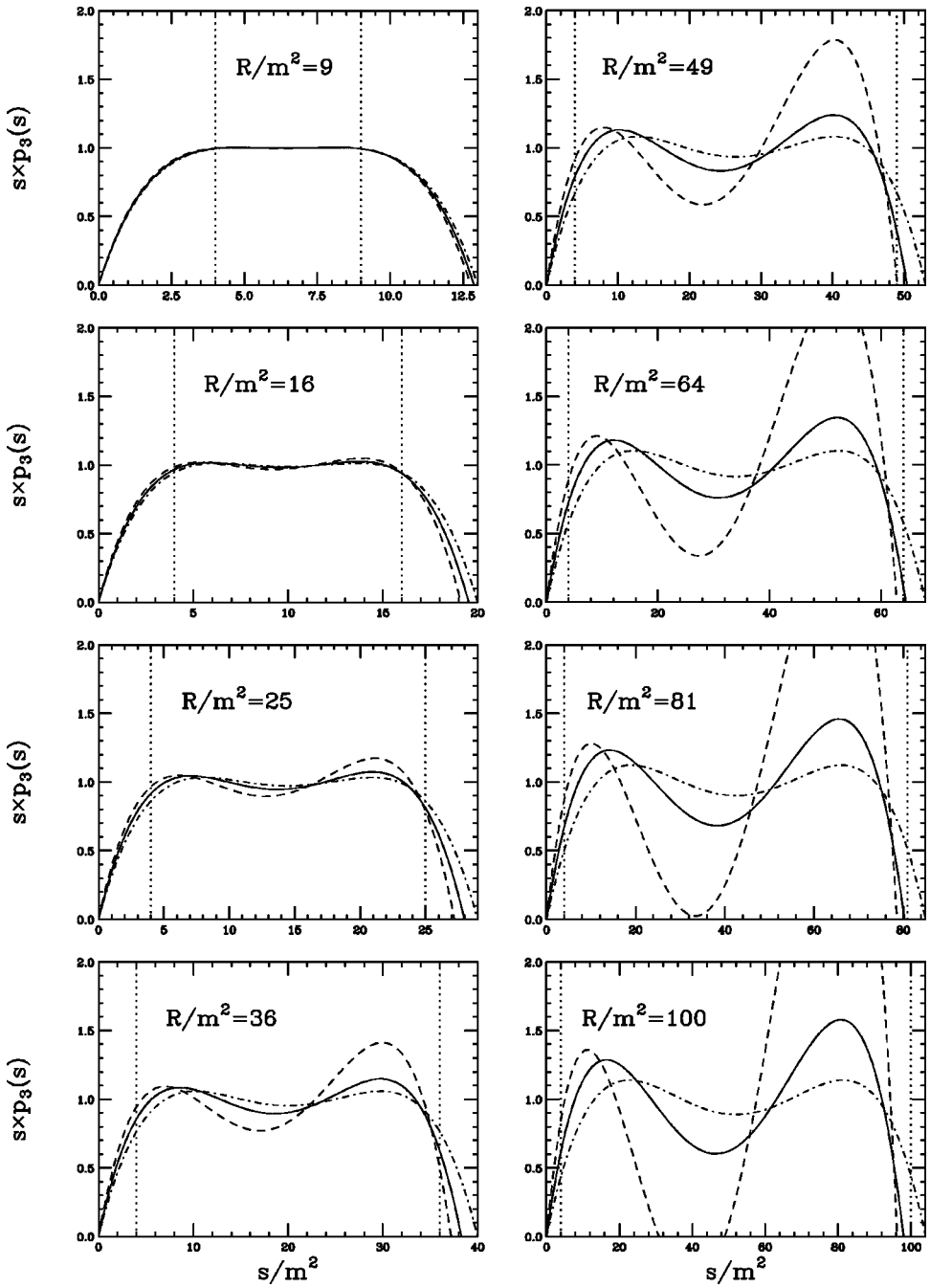

FIG. 3. The cubic fit for various choices of the UV cutoff R. The IR cutoff is fixed at $s_0/m^2=4$. The ratio $s\times p_3(s)$ is shown for the P_n fit (solid line), the T_n fit (dashed line), and the U_n fit (dot-dashed line). The vertical dotted lines indicate the upper and lower limits of the fit interval.

2. ACD technique: Perturbative spectral function

Let us now use the ACD technique to calculate $S_{\rm pert}$ to see if $1/6\pi$ can be reproduced.

We begin by choosing the integration interval $[s_0,R]$. The choice for the lower limit of the interval is clear. It is $s_0=4m^2$. The upper limit R is arbitrary. We will let it vary between $R=9m^2$ and $R=100m^2$. For the fit routine, we will use the least squares fit (P_n fit), the minimax fit (T_n fit), and the least-first-power fit (U_n fit), and check the routine dependence of the results.

Typical results of the fits for various choices of the UV cutoff R using the three fit routines are shown in Fig. 3. The value of the fit error $\delta S_{\rm fit}(N)$ was calculated analytically using the formulas in Appendix C and the results are shown in Fig. 4. As is evident from Fig. 4, the fit error is well under control for the 1-loop perturbative spectral function even for $R/m^2=100$. In particular, the least-squares fit shows the fastest convergence for all cases with excellent agreement achieved at $N=3$.

This excellent control on the fit error can be understood as due to the spread out and positive definite nature of the perturbative spectral functions. The error from where the polynomial undershoots $1/s$ tends to be canceled by the error from where the polynomial overshoots it. This is in stark contrast to the δ-function model, to be considered in the next subsection, where due to the localized nature of the spectral function, the fit error oscillates several times before converging to zero as N is increased.

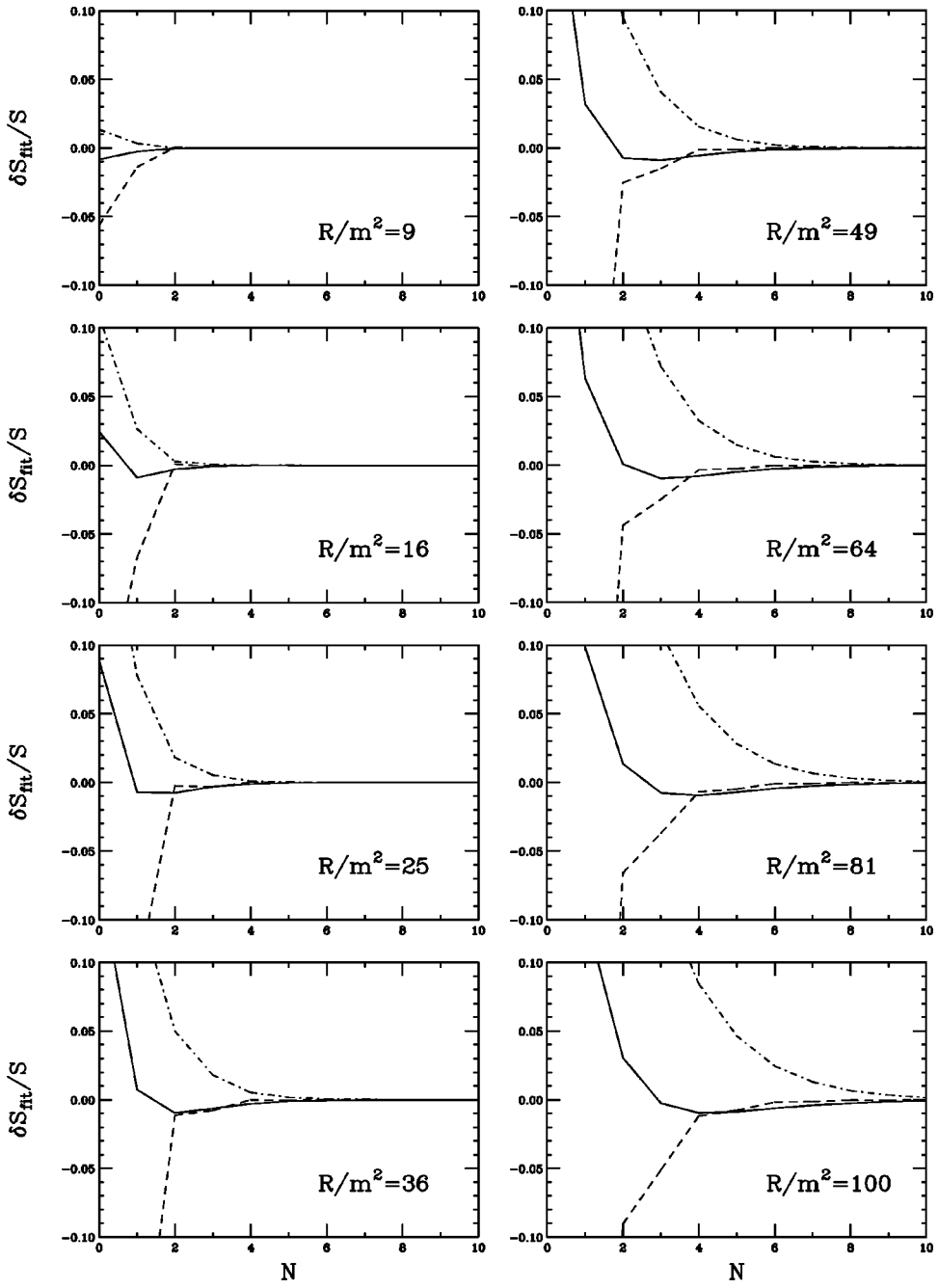

FIG. 4. The dependence of the fit error on the order of the polynomial N. The IR cutoff is fixed at $s_0/m^2=4$ while the UV cutoff R/m^2 is varied. The results are shown for the P_n fit (solid line), the T_n fit (dashed line), and the U_n fit (dot-dashed line).

Next, we evaluate the truncation error. The large momentum expansion of Eq. (7.1) is given in Appendix B. $\delta S_{\rm trunc}$ can be calculated analytically using the formulas of Appendix C. The results are shown in Fig. 5 for the least-squares fit. We find that the truncation error is also well under control.

Finally, we calculate the analytic continuation error. Here, we encounter a disaster. Figure 6 shows the value of $S_{\rm ACD}$ as a function of N and we see that $S_{\rm ACD}$ actually diverges: neglecting the s dependence of the $h_n(s)$'s fails miserably as an approximation. The reason for this can be traced to the fact that even though the difference $1/s-p_N(s)$ converges to zero within its radius of convergence, outside it diverges [cf. Eq. (5.1)]. The error induced by the neglect of the s dependence of the $h_n(s)$'s may be suppressed near the real s axis, but it is actually *enhanced* away from it.

What we have found here is that even though the fit and truncation errors are well under control, the analytic continuation error is not.

B. Vector meson dominance I: δ-function model

Next, let us consider the following vector meson dominance model where the vector and axial-vector channels are each saturated by a single vector meson pole:

$$\mathcal{F}_{\rm V}(s)=f_{\rm V}^2\frac{1}{s-m_{\rm V}^2+i\epsilon},$$

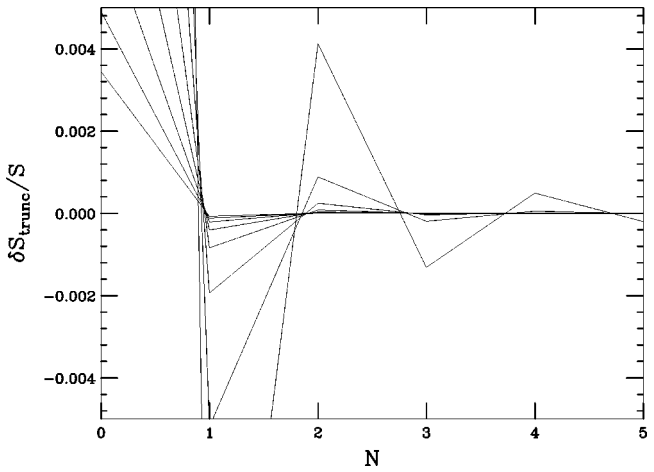

FIG. 5. The dependence of the truncation error on the order of the polynomial N and the UV cutoff R. The IR cutoff is fixed at $s_0/m^2=4$. The results are shown for $R/m^2=9$, 16, 25, 36, 49, 64, 81, and 100, with larger values of R showing faster convergence. The fit routine used was the P_n fit.

$$\mathcal{F}_A(s)=f_A^2\frac{1}{s-m_A^2+i\epsilon}.$$

The value of S in this case is

$$S=-4\pi[\mathcal{F}_V(0)-\mathcal{F}_A(0)]=4\pi\left[\frac{f_V^2}{m_V^2}-\frac{f_A^2}{m_A^2}\right]. \quad (7.4)$$

1. Dispersion relation: δ-function model

The imaginary parts of $\mathcal{F}_V(s)$ and $\mathcal{F}_A(s)$ are

$$\mathrm{Im}\,\mathcal{F}_V(s)=-\pi f_V^2\delta(s-m_V^2),$$

$$\mathrm{Im}\,\mathcal{F}_A(s)=-\pi f_A^2\delta(s-m_A^2).$$

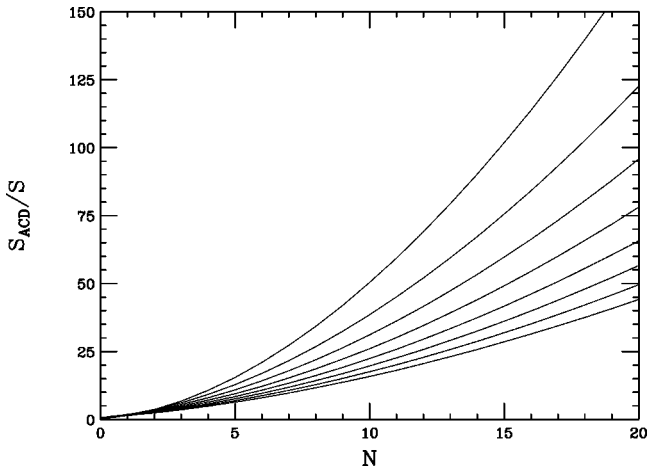

FIG. 6. The ACD estimate of S for the perturbative spectral function using the P_n fit. The IR cutoff is fixed at $s_0/m^2=4$ while the UV cutoff was given the values $R/m^2=9$, 16, 25, 36, 49, 64, 81, and 100. Smaller values of R showed faster divergence.

Using Eq. (3.2) recovers Eq. (7.4) as follows:

$$S=4\pi\int_0^\infty\frac{ds}{s}[f_V^2\delta(s-m_V^2)-f_A^2\delta(s-m_A^2)]$$

$$=4\pi\left[\frac{f_V^2}{m_V^2}-\frac{f_A^2}{m_A^2}\right]. \quad (7.5)$$

The Weinberg sum rules, Eq. (3.3), impose the following conditions on the decay constants and masses:

$$f_V^2-f_A^2=f_{TC}^2,$$

$$m_V^2f_V^2-m_A^2f_A^2=0. \quad (7.6)$$

Solving for the decay constants, we obtain

$$f_V^2=\frac{1}{1-r}f_{TC}^2,\quad f_A^2=\frac{r}{1-r}f_{TC}^2,\quad r\equiv\frac{m_V^2}{m_A^2}.$$

Then,

$$S=4\pi(1+r)\frac{f_{TC}^2}{m_V^2}. \quad (7.7)$$

In the leading large-N approximation, we can relate the necessary ratios to their QCD counterparts as

$$\frac{f_{TC}^2}{m_V^2}\approx\frac{f_\pi^2}{m_\rho^2}\frac{N_D N_{TC}}{3}\approx 0.005\,N_D N_{TC},$$

$$r=\frac{m_V^2}{m_A^2}\approx\frac{m_\rho^2}{m_{a_1}^2}\approx 0.4. \quad (7.8)$$

Then,

$$S\approx 0.09\,N_D N_{TC}, \quad (7.9)$$

which agrees with Eq. (3.5).

2. ACD technique: δ-function model

We now turn to the ACD technique to see if Eq. (7.7) can be reproduced. We fix the value of the ratio $r=m_V^2/m_A^2$ to the large-N value $r=0.4$. The integration interval $[s_0,R]$ is chosen to include both resonances. We take various combinations of $s_0/m_V^2=0.5,0.25,0.125$ and $R/m_V^2=4,8,16$. For the fit routine, we again consider the least squares fit (P_n fit), the least-first-power fit (U_n fit), and the minimax fit (T_n fit).

The large momentum expansion for this model is very simple:

$$\mathcal{F}(s)=\sum_{n=0}^\infty\frac{f_V^2m_V^{2n}-f_A^2m_A^{2n}}{s^{n+1}}=\frac{f_{TC}^2}{s}+\sum_{n=2}^\infty\frac{f_{TC}^2m_V^{2n}}{s^{n+1}}X_{2n}(r),$$

where

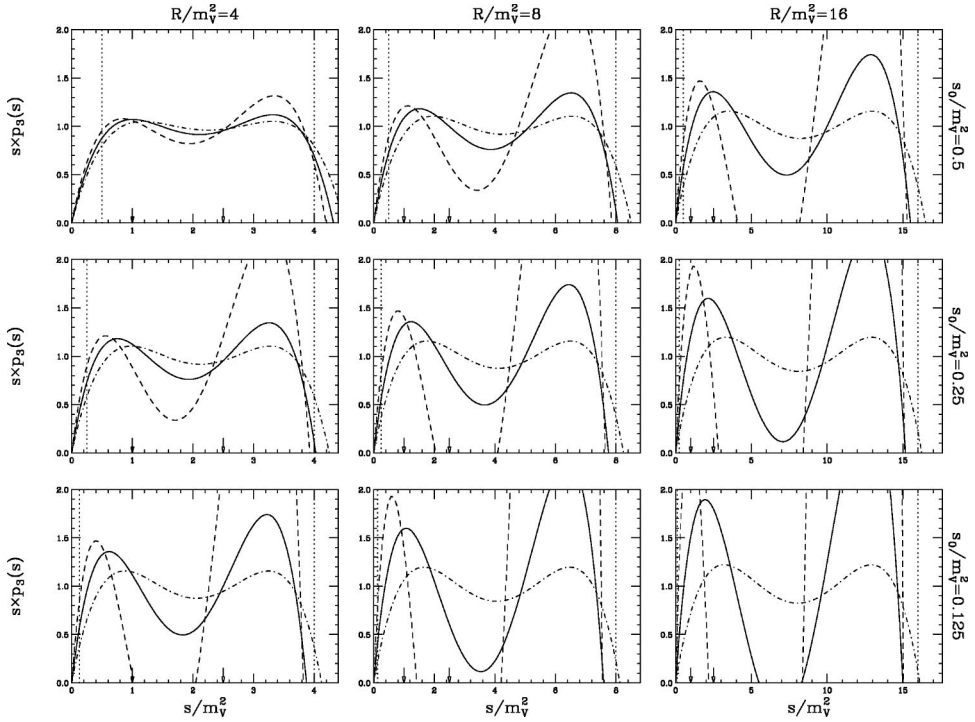

FIG. 7. The cubic polynomial fit to $1/s$ for various combinations of $s_0/m_V^2=0.5,0.25,0.125$ and $R/m_V^2=4,8,16$. The product $s\times p_3(s)$ is shown for the least-squares fit (solid line), the least-first-power fit (dot-dashed line), and the minimax fit (dashed line). The positions of the δ-function resonances are shown with arrows on the s axis. The vertical dotted lines show the upper and lower limits of the fit interval.

$$X_n(r)\equiv\left(\frac{1-r^{1-n/2}}{1-r}\right). \tag{7.10}$$

This series is obviously convergent for $s>m_{\rm A}^2$.

Note that the coefficients of this expansion carry no s dependence. Therefore, the analytic continuation error and the truncation error (for $M>N$) are both automatically zero and the fit error will be the sole source of error.

The fit error is easy to calculate. Since the imaginary part of $\mathcal{F}(s)$ is just two δ functions, $\delta S_{\rm fit}$ is given by

$$\delta S_{\rm fit}=4\pi\int_{s_0}^{R}ds\left[\frac{1}{s}-p_N(s)\right][f_{\rm V}^2\delta(s-m_{\rm V}^2)-f_{\rm A}^2\delta(s-m_{\rm A}^2)]$$
$$=4\pi f_{\rm V}^2\left[\frac{1}{m_{\rm V}^2}-p_N(m_{\rm V}^2)\right]-4\pi f_{\rm A}^2\left[\frac{1}{m_{\rm A}^2}-p_N(m_{\rm A}^2)\right].$$

In Fig. 7 we show the quality of cubic polynomial fits for various combination of the IR and UV cutoffs for the three fit routines mentioned above. As is evident from this figure, the quality of the fit degrades quickly as the fit interval is increased. It is also highly routine dependent. The dependence of the ratio $\delta S_{\rm fit}/S_{\rm exact}$ for various choices of the interval $[s_0,R]$, the order of the polynomial N, and the fit routine is shown in Fig. 8.

Notice that in contrast to the perturbative spectral function case discussed in the previous subsection, the fit error oscillates several times before converging to zero. This can be understood as follows: In the present case under consideration, $\mathrm{Im}\,\mathcal{F}(s)$ is a superposition of δ functions. If a node of $1/s-p_N(s)$ coincides with the position of a δ function, then the contribution to the fit error from that δ function is zero. As the order of the fit polynomial is increased, the nodes of $1/s-p_N(s)$ will move through the δ functions, leading to the oscillatory behavior of $\delta S_{\rm fit}$ seen here.

When the fit interval $[s_0,R]$ is small, the convergence is good for all three fit routines and the fit error is well under control. However, choosing a small fit interval requires prior knowledge of where the relevant structure of the spectral function is localized. Without this knowledge, we have no guideline as to how the fit interval should be chosen, and if we take it to be too large, the oscillations can persist beyond $N=10$ as can be seen from Fig. 8 and it will be difficult to tell whether convergence has been reached.

C. Vector meson dominance II: Breit-Wigner model

We have seen from the previous subsection that when the ACD technique is applied to a highly localized spectral function, the fit error is difficult to control. On the other hand, for a smooth, slowly varying spectral function, it was the analytic continuation error which was problematic. In this section, we consider a function which can interpolate between the two extreme cases to see whether a balance can be achieved where both $\delta S_{\rm fit}$ and $\delta S_{\rm AC}$ are under control.

The model function we consider here has a Breit-Wigner type imaginary part on the real s axis and the correct analyticity in the complex s plane:

$$\mathcal{F}_{\rm V}(s)=f_{\rm V}^2\frac{1}{s-m_{\rm V}^2+i\sqrt{s}\Gamma_{\rm V}},$$

$$\mathcal{F}_{\rm A}(s)=f_{\rm A}^2\frac{1}{s-m_{\rm A}^2+i\sqrt{s}\Gamma_{\rm A}}.$$

In the limit $\Gamma_{\rm V},\Gamma_{\rm A}\to+0$, these functions reduce to the previous δ-function model. In the other limit where $\Gamma_{\rm V}$ and $\Gamma_{\rm A}$

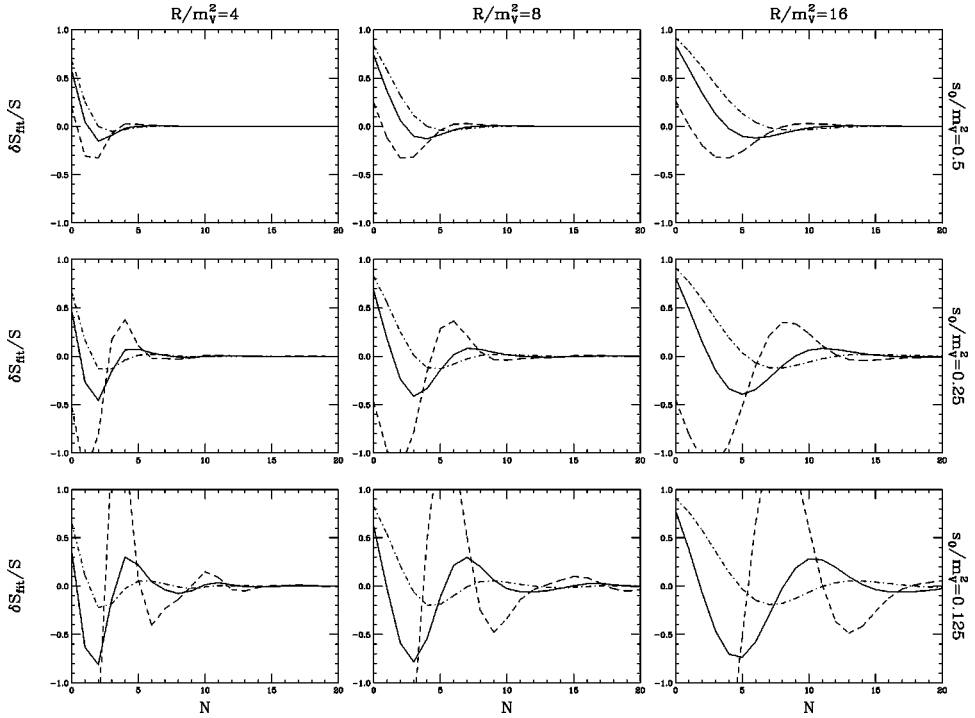

FIG. 8. The dependence of the fit error on the order of the fit polynomial N. Results for the least-squares fit (solid line), the least-first-power fit (dot-dashed line), and the minimax fit (dashed line) are shown.

are of the same order as m_V and m_A, we obtain a smooth function reminiscent of the perturbative case. This is shown in Fig. 9.

The expression for S in terms of the vector meson masses and decay constant is the same as the δ function case:

$$S=-4\pi[\mathcal{F}_V(0)-\mathcal{F}_A(0)]=4\pi\left[\frac{f_V^2}{m_V^2}-\frac{f_A^2}{m_A^2}\right]. \quad (7.11)$$

1. Dispersion relation: Breit-Wigner model

The imaginary parts are now given by

$$\mathrm{Im}\,\mathcal{F}_V(s)=-f_V^2\frac{\sqrt{s}\Gamma_V}{(s-m_V^2)^2+s\Gamma_V^2}\theta(s),$$

$$\mathrm{Im}\,\mathcal{F}_A(s)=-f_A^2\frac{\sqrt{s}\Gamma_A}{(s-m_A^2)^2+s\Gamma_A^2}\theta(s). \quad (7.12)$$

It is straightforward to check that

$$f^2\int_0^\infty\frac{ds}{s}\frac{\sqrt{s}\Gamma}{(s-m^2)^2+s\Gamma^2}=\frac{f^2}{m^2}\int_0^\infty dx\frac{\xi}{(x^2-1)^2+x^2\xi^2}$$

$$=\pi\frac{f^2}{m^2},$$

where

$$x=\frac{\sqrt{s}}{m},\quad \xi=\frac{\Gamma}{m}, \quad (7.13)$$

from which we can and see that Eq. (7.11) is recovered in Eq. (3.2).

The constraint from the first Weinberg sum rule is given by

$$f_V^2-f_A^2=f_{TC}^2, \quad (7.14)$$

as before. The integral for the second Weinberg sum rule does not converge. However, if we recall that the second Weinberg sum rule is related to the non-appearance of a dimension 4 operator in the OPE of $\mathcal{F}(-Q^2)$, we can impose the conditions

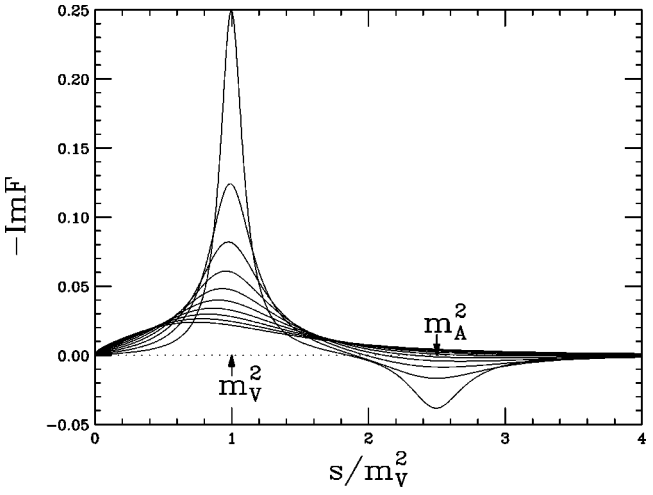

FIG. 9. The spectral functions for the Breit-Wigner model. The ratio $\xi\equiv\Gamma_V/m_V=\Gamma_A/m_A$ is varied from $\xi=0.1$ to $\xi=1.0$ at 0.1 intervals with smaller values of ξ corresponding to more prominent peaks. The arrows indicate the positions of the techni-ρ and techni-a_1 peaks.

$$f_V^2 m_V^2 - f_A^2 m_A^2 = 0,$$

$$f_V^2 \Gamma_V^2 - f_A^2 \Gamma_A^2 = 0, \tag{7.15}$$

which has the desired effect of making the coefficient of $1/Q^4$ vanish and make the large momentum expansion of this toy model mimic that of QCD. Since Eqs. (7.14) and (7.15) are the same as Eq. (7.6) with the extra condition

$$\frac{m_V^2}{m_A^2} = \frac{\Gamma_V^2}{\Gamma_A^2} = r \quad \text{or} \quad \frac{\Gamma_V}{m_V} = \frac{\Gamma_A}{m_A} \equiv \xi,$$

the estimate of S remains unchanged from Eq. (7.9).

Note that the value of S is independent of the ratio $\xi \equiv \Gamma_V/m_V = \Gamma_A/m_A$. However, the shape of the spectral function $\mathrm{Im}\,\mathcal{F}(s)$ is not. In Fig. 9, we show the shape of the spectral function for various choices of ξ. For the $N_D = 1, N_{TC} = 3$ case, the value of ξ using the large-N relation is

$$\xi = \frac{\Gamma_V}{m_V} \approx \frac{\Gamma_\rho}{m_\rho} \approx 0.2.$$

2. ACD technique: Breit-Wigner model

The large momentum expansion of our model function is given by

$$\begin{aligned} f^2 \frac{1}{s - m^2 + i\xi m\sqrt{s}} &= \frac{f^2}{s} \sum_{n=0}^{\infty} U_n(\xi/2) \left(-i \frac{m}{\sqrt{s}} \right)^n \\ &= \frac{f^2}{s} \sum_{n=0}^{\infty} \frac{(-1)^n m^{2n}}{s^n} \left[U_{2n}(\xi/2) - i \frac{m}{\sqrt{s}} U_{2n+1}(\xi/2) \right] \\ &= \frac{f^2}{s} + \frac{f^2}{s} \sum_{n=0}^{\infty} \frac{(-1)^n m^{2n}}{s^n} \left[U_{2n}(\xi/2) \right. \\ &\quad \left. + i \frac{\sqrt{s}}{m} U_{2n-1}(\xi/2) \right], \end{aligned}$$

where $U_n(\cos\theta) = \sin(n+1)\theta/\sin\theta$ are the Chebyshev polynomials of the second kind.[6] In the limit $\xi \to +0$, we find $U_{2n}(0) = (-1)^n$ and $U_{2n-1}(0) = 0$ and all the half-integer power terms vanish. Note that there is an ambiguity in treating the half-integer power terms since we can consider it as a coefficient of either the next higher integer power term with a $\sqrt{s}$ behavior or the next lower integer power term with an $1/\sqrt{s}$ behavior.

Imposing the conditions of Eqs. (7.14) and (7.15), we find

$$\begin{aligned} \mathcal{F}(s) &= \frac{f_{TC}^2}{s} \sum_{n=0}^{\infty} \frac{(-1)^n m_V^{2n}}{s^n} \left[X_{2n}(r) U_{2n}(\xi/2) \right. \\ &\quad \left. - i \frac{m_V}{\sqrt{s}} X_{2n+1}(r) U_{2n+1}(\xi/2) \right] \\ &= \frac{f_{TC}^2}{s} \left[1 - i \frac{m_V}{\sqrt{s}} X_1(r) U_1(\xi/2) \right] \\ &\quad + \frac{f_{TC}^2}{s} \sum_{n=2}^{\infty} \frac{(-1)^n m_V^{2n}}{s^n} \left[X_{2n}(r) U_{2n}(\xi/2) \right. \\ &\quad \left. + i \frac{\sqrt{s}}{m_V} X_{2n-1}(r) U_{2n-1}(\xi/2) \right] \end{aligned} \tag{7.16}$$

where $X_n(r)$ is defined as in Eq. (7.10):

$$X_n(r) \equiv \frac{1 - r^{1-n/2}}{1 - r}.$$

In order to make the $1/s^2$ term vanish completely, we have associated the $1/s^{3/2}$ term with the $1/s$ term and the $1/s^{n+1/2}$ term with the $1/s^{n+1}$ term for $n \geq 2$.[7]

We have a slight problem with the choice of fit interval since our model function has a branch cut which begins at $s = 0$ but the IR cutoff s_0 must be kept non-zero. In order to circumvent this problem, we divide the dispersion relation integral of S into two pieces:

$$S = S_{IR}(s_0) + S_{UV}(s_0)$$

where

$$S_{IR}(s_0) = -4 \int_0^{s_0} \frac{ds}{s} \mathrm{Im}\,\mathcal{F}(s)$$

$$S_{UV}(s_0) = -4 \int_{s_0}^{\infty} \frac{ds}{s} \mathrm{Im}\,\mathcal{F}(s).$$

The IR piece of the dispersion integral, $S_{IR}(s_0)$, is then calculated using the exact form of the spectral function given in Eq. (7.12), while the ACD technique is applied only to the UV piece $S_{UV}(s_0)$.

The evaluation of $S_{UV}(s_0)$ amounts to replacing the function $\theta(s)$ in the spectral function with $\theta(s - s_0)$ so that the branch cut is shifted to start from s_0. The coefficients of the large momentum expansion in Eq. (7.16) must be adjusted accordingly:

[6] The Chebyshev polynomials of the second kind $U_n(x)$ are the same thing as the Gegenbauer polynomials $C_n^\nu(x)$ with $\nu = 1$. See Appendix A 3 and Ref. [24].

[7] If we associate all the $1/s^{n+1/2}$ terms with the $1/s^n$ terms so that all the coefficients $h_n(s)$ have a $1/\sqrt{s}$ behavior, then it is possible to prove that the value of S_{ACD} (without any IR subtraction) in the resulting model converges to the correct value of S when ξ is small even though the truncation and analytical continuation errors both diverge. Such conspiration between the two errors is not common and we consider this to be a pathological case.

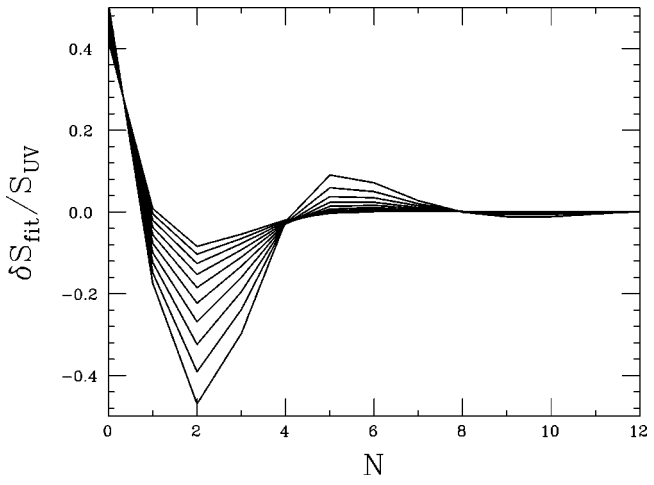

FIG. 10. The N dependence of the fit error for the Breit-Wigner model. The ratio $\xi \equiv \Gamma_V/m_V = \Gamma_A/m_A$ is varied from $\xi = 0.1$ to $\xi = 1.0$ at 0.1 intervals. Larger values of ξ show faster convergence.

$$h_m(s) \to h_m(s) - \delta h_m$$

where

$$\delta h_m = -\frac{1}{\pi}\int_0^{s_0} ds\, s^m \,\mathrm{Im}\,\mathcal{F}(s).$$

In our previous paper [18], we used an approximate form of the spectral function to calculate S_{IR} and the shifts in the large momentum expansion coefficients δh_m. However, we have discovered that this approximation introduced yet another source of error into our analysis and that our results in Ref. [18] were in fact totally unreliable.[8] In this paper, we used the exact forms of the spectral functions to calculate both S_{IR} and the δh_m's analytically using the formulas in Appendix D.

This partial use of the dispersion relation and the use of the exact spectral functions in the infrared do not go against ACD philosophy since, in actual technicolor models, only the Goldstone and pseudo Goldstone bosons are dynamical at low energy and their contribution to the spectral functions can be calculated using standard chiral Lagrangian techniques.

In the following, we present our ACD evaluation of S_{UV} with $s_0/m_V^2 = 0.2$, and $R/m_V^2 = 5$. The fit routine used will be the least-squares fit (P_n-fit). We will assume $r = m_V^2/m_A^2 = \Gamma_V^2/\Gamma_A^2 = 0.4$, and let the ratio $\xi \equiv \Gamma_V/m_V = \Gamma_A/m_A$ vary.

In Fig. 10, we show the N dependence of the fit error. Different lines correspond to different values of the ratio $\xi = \Gamma_V/m_V = \Gamma_A/m_A$ which was varied from $\xi = 0.1$ to $\xi = 1.0$ in 0.1 intervals. As was expected, the fit error converges faster for larger values of ξ which correspond to spectral functions which are more spread out. For the QCD-like $\xi = 0.2$ case, one needs $N \geqslant 4$ for the fit error to be within 10%.

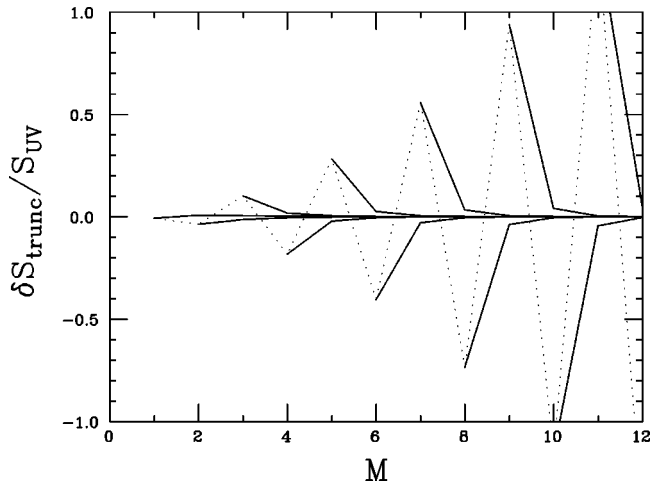

FIG. 11. The M dependence of the truncation error for the Breit-Wigner model with $\xi = 0.2$. The points connected by solid lines are the errors for the same order of the polynomial N. The dotted line connects the points where $M = N+1$.

In Fig. 11, we show the M dependence of the truncation error for fixed values of N with $\xi = 0.2$. As expected, the truncation error converges rapidly for each fixed value of N. However, an unexpected result is that if one looks at the N dependence of the truncation error for the $M = N+1$ case, it diverges. This means that increasing the order of the polynomial does not necessarily decrease the truncation error. Rather, one must keep the order of the polynomial fixed and increase the number of terms retained in the large momentum expansion. This result is independent of the value we choose for ξ as can be seen in Fig. 12.

Finally, the N dependence of the analytic continuation error is shown in Fig. 13. The analytic continuation error for

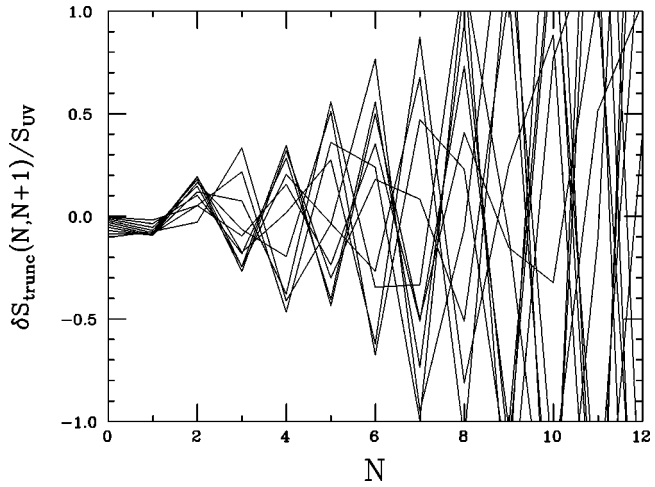

FIG. 12. The N dependence of the truncation error $\delta S_{trunc}(N,N+1)$ for the Breit-Wigner model. The ratio $\xi \equiv \Gamma_V/m_V = \Gamma_A/m_A$ is varied from $\xi = 0.1$ to $\xi = 1.0$ at 0.1 intervals. There is no discernible pattern relating the behavior of the error to the value of ξ.

[8] We also discovered a bug in our program which resulted in giving a $1/\sqrt{s}$ dependence to the coefficients $h_m(s)$, contrary to what was reported in Ref. [18].

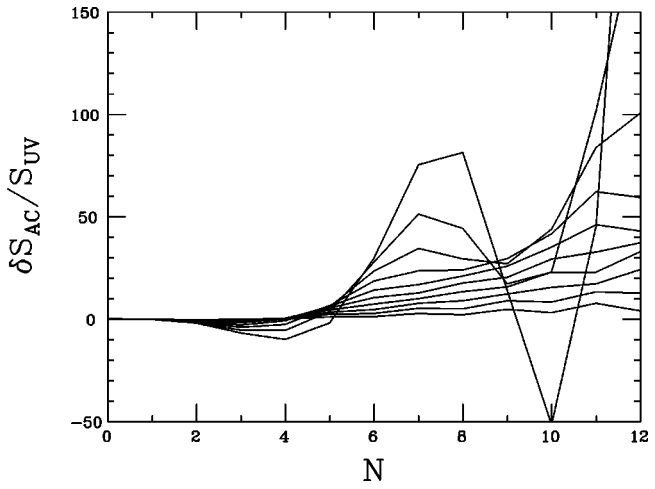

FIG. 13. The N dependence of the analytic continuation error for the Breit-Wigner model. The ratio $\xi \equiv \Gamma_V/m_V = \Gamma_A/m_A$ is varied from $\xi = 0.1$ to $\xi = 1.0$ at 0.1 intervals. Smaller values of ξ show slower divergence.

smaller values of ξ shows slower divergence as expected, but still diverges eventually. A closeup of Fig. 13 is shown in Fig. 14. Even for the smallest value of ξ we considered, namely $\xi = 0.1$, the analytic continuation error quickly diverges beyond control above and including $N = 5$.

The result of this subsection is discouraging. By comparing Figs. 10 and 14, it is evident that there is no intermediate value of ξ for which both the fit error and analytic continuation error are under control. Furthermore, we have discovered that in order to control the truncation error, contrary to expectation, we must increase the number of terms retained in the large momentum expansion M without increasing the order of the polynomial N.

D. Shifman model

In the δ-function and Breit-Wigner models considered in the previous subsections, both the vector and axial-vector spectral functions were each saturated by a single meson pole. In this and the following subsection, we will look at models in which an infinite ladder of poles contribute to each channel. The models differ from each other in the spacing of the poles.

The model we consider in this subsection was introduced by Shifman in Ref. [22]. Using the di-gamma function $\psi(z)$ given by

$$\psi(z) = \frac{d}{dz}\ln\Gamma(z) = \frac{\Gamma'(z)}{\Gamma(z)} = -\gamma_E - \sum_{n=0}^{\infty}\left(\frac{1}{z+n} - \frac{1}{1+n}\right),$$

where $-\psi(1) = \gamma_E$ is Euler's constant, we define

$$\mathcal{F}_V(s) = f_V^2\frac{\psi(1-s/m_V^2)-\psi(1)}{s} = \sum_{k=1}^{\infty}\frac{f_V^2}{k}\frac{1}{s-km_V^2},$$

$$\mathcal{F}_A(s) = f_A^2\frac{\psi(1-s/m_A^2)-\psi(1)}{s} = \sum_{k=1}^{\infty}\frac{f_A^2}{k}\frac{1}{s-km_A^2}.$$

These functions can be interpreted as infinite sums over spin 1 meson poles of masses $\sqrt{k}m_{V,A}$ and decay constants $f_{V,A}/\sqrt{k}$ where k is an integer.

The value of S in this case is

$$S = 4\pi\psi'(1)\left[\frac{f_V^2}{m_V^2} - \frac{f_A^2}{m_A^2}\right], \quad \psi'(1) = \zeta(2) = \frac{\pi^2}{6}. \tag{7.17}$$

1. Dispersion relation: Shifman model

The imaginary parts of $\mathcal{F}_V(s)$ and $\mathcal{F}_A(s)$ are

$$\mathrm{Im}\,\mathcal{F}_V(s) = -\pi f_V^2\sum_{k=1}^{\infty}\frac{1}{k}\delta(s-km_V^2),$$

$$\mathrm{Im}\,\mathcal{F}_A(s) = -\pi f_A^2\sum_{k=1}^{\infty}\frac{1}{k}\delta(s-km_A^2).$$

Using Eq. (3.2), we recover Eq. (7.17):

$$S = 4\pi\left[\frac{f_V^2}{m_V^2} - \frac{f_A^2}{m_A^2}\right]\sum_{k=1}^{\infty}\frac{1}{k^2} = 4\pi\zeta(2)\left[\frac{f_V^2}{m_V^2} - \frac{f_A^2}{m_A^2}\right].$$

The first and second Weinberg sum rules cannot be imposed on this model because both integrals diverge except in the trivial limit $f_V = f_A$ and $m_V = m_A$ in which case $S = 0$. We will nevertheless impose the condition

$$m_V^2 f_V^2 - m_A^2 f_A^2 = 0 \tag{7.18}$$

which has the effect of making the $1/s^2$ term in the OPE of $\mathcal{F}(s)$ vanish as required by chiral symmetry. We emphasize here that this model is a toy model which is not motivated by any particular field theory. The condition imposed here is simply to make our model as a mock-up of QCD. We also denote

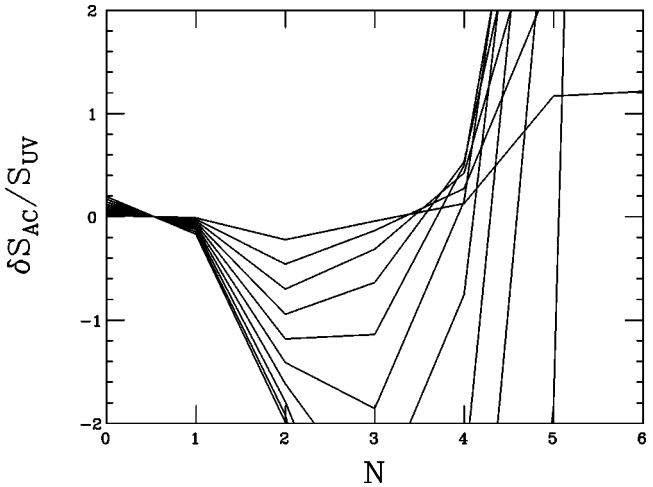

FIG. 14. Closeup of Fig. 13. The ratio $\xi \equiv \Gamma_V/m_V = \Gamma_A/m_A$ is varied from $\xi = 0.1$ to $\xi = 1.0$ at 0.1 intervals. Smaller values of ξ show slower divergence.

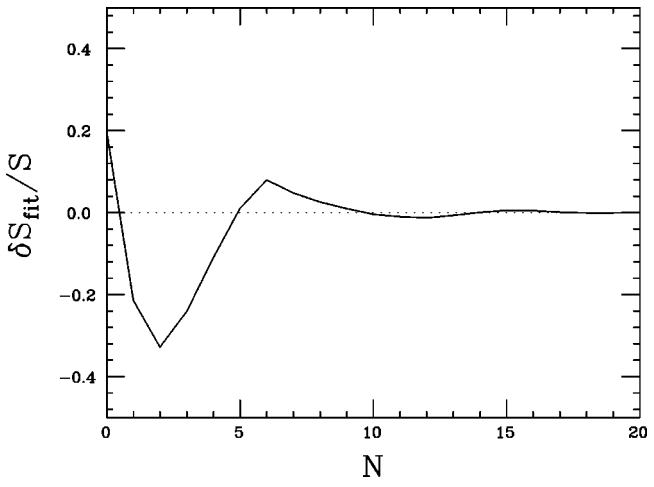

FIG. 15. The N dependence of the fit error for the Shifman model.

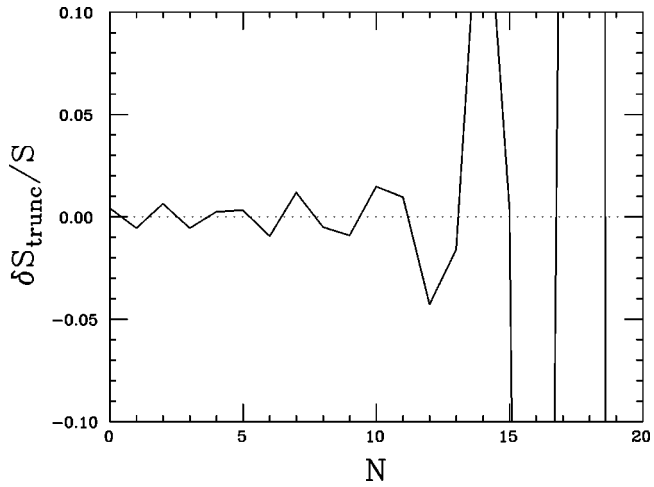

FIG. 16. The N dependence of the truncation error for the Shifman model.

$$f_{\rm V}^2 - f_{\rm A}^2 = f_*^2 .$$

Then,

$$f_{\rm V}^2 = \frac{1}{1-r} f_*^2 , \quad f_{\rm A}^2 = \frac{r}{1-r} f_*^2 , \quad r = \frac{m_{\rm V}^2}{m_{\rm A}^2},$$

and

$$S = 4\pi\zeta(2)(1+r)\frac{f_*^2}{m_{\rm V}^2}.$$

There is no simple way to relate f_* to $f_{\rm TC}$ since the coefficient of $1/s$ in the large momentum expansion of this model diverges logarithmically for both $s \to 0$ and $s \to \infty$.

2. ACD technique: Shifman model

The large momentum expansion of $\mathcal{F}(s)$ can be obtained using the following asymptotic form of the di-gamma function $\psi(z)$:

$$\psi(z) \sim \ln(z-1) + \frac{1}{2(z-1)} + \sum_{n=1}^{M} \frac{(-1)^n B_n}{2n} \frac{1}{(z-1)^{2n}}, \tag{7.19}$$

where B_n are the Bernoulli numbers. Note that, unlike the previous cases, this is not a convergent series but an asymptotic one. In particular, the coefficients of the expansion increase like $n!$. Recalling that $\psi(1) = -\gamma_E$, we find

$$\mathcal{F}_{\rm V}(s) \sim f_{\rm V}^2 \left[\frac{\gamma_E + \ln(-s/m_{\rm V}^2)}{s} - \frac{m_{\rm V}^2}{2s^2} + \sum_{n=1}^{M} \frac{(-1)^n B_n}{2n} \frac{m_{\rm V}^{4n}}{s^{2n+1}} \right],$$

$$\mathcal{F}_{\rm A}(s) \sim f_{\rm A}^2 \left[\frac{\gamma_E + \ln(-s/m_{\rm A}^2)}{s} - \frac{m_{\rm A}^2}{2s^2} + \sum_{n=1}^{M} \frac{(-1)^n B_n}{2n} \frac{m_{\rm A}^{4n}}{s^{2n+1}} \right],$$

and

$$\mathcal{F}(s) = \frac{(f_{\rm V}^2 - f_{\rm A}^2)\gamma_E + [f_{\rm V}^2 \ln(-s/m_{\rm V}^2) - f_{\rm A}^2 \ln(-s/m_{\rm A}^2)]}{s} + \sum_{n=1}^{M} \frac{(-1)^n B_n}{2n} \frac{f_{\rm V}^2 m_{\rm V}^{4n} - f_{\rm A}^2 m_{\rm A}^{4n}}{s^{2n+1}}$$

$$= \frac{f_*^2 [g(R, m_{\rm V}, m_{\rm A}) + \ln(-s/R)]}{s} + \sum_{n=1}^{M} \frac{f_*^2 m_{\rm V}^{4n}}{s^{2n+1}} \left[\frac{(-1)^n B_n}{2n} X_{4n}(r) \right],$$

where

$$g(R, m_{\rm V}, m_{\rm A}) = \gamma_E + \frac{1}{2}\ln\frac{R}{m_{\rm V}^2} + \frac{1}{2}\ln\frac{R}{m_{\rm A}^2} - \frac{1}{2}\left(\frac{m_{\rm A}^2 + m_{\rm V}^2}{m_{\rm A}^2 - m_{\rm V}^2} \right) \ln\frac{m_{\rm V}^2}{m_{\rm A}^2}.$$

In this case, only h_1 is s dependent, and the $1/s^2$ term has vanished due to Eq. (7.18), leaving only the odd power terms.

For the fit interval, we chose $s_0/m_{\rm V}^2 = 0.2$ and $R/m_{\rm V}^2 = 6.5$. This placed 6 vector resonances and 2 axial-vector resonances within the fit interval. The fit routine was the least-squares fit, and $r = m_{\rm V}^2/m_{\rm A}^2 = 0.4$. The results are shown in Figs. 15–17. The fit and analytical continuation errors show the standard expected behavior: the fit error converges while the analytical continuation error diverges.

The truncation error shown is calculated for $M = N+1$. Since only the first coefficient h_1 has any s dependence, including more than $M = N+1$ terms in the large momentum

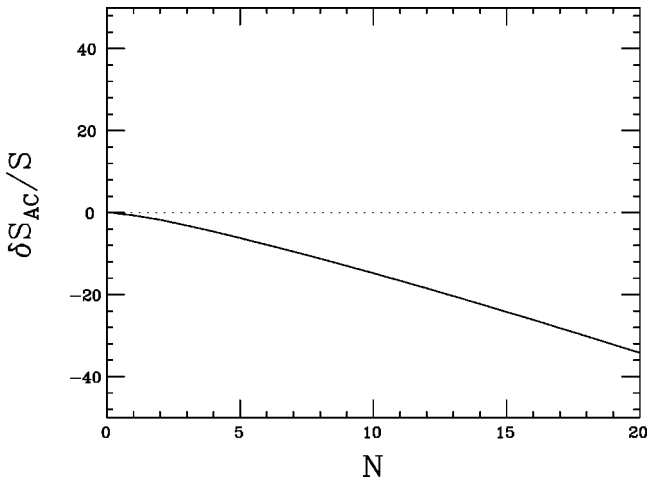

FIG. 17. The N dependence of the analytic continuation error for the Shifman model.

expansion has no effect on the truncation error. The eventual divergence of the truncation error is as expected since the large momentum expansion of the Shifman model is asymptotic and not convergent as was the case with the previous models. However, it does stay within the $\sim 1\%$ range up to about $N=11$.

E. Cotangent model

An infinite ladder of resonances does not necessarily lead to an asymptotic expansion. Using the following convergent expansion of the cotangent function,

$$\frac{\pi}{2z}\cot \pi z - \frac{1}{2z^2} = \sum_{n=1}^{\infty} \frac{1}{z^2-n^2},$$

we define

$$\mathcal{F}_{\rm V}(s) = \frac{f_{\rm V}^2}{m_{\rm V}^2}\left[\frac{\pi m_{\rm V}}{2\sqrt{s}}\cot\left(\frac{\pi\sqrt{s}}{m_{\rm V}}\right) - \frac{m_{\rm V}^2}{2s}\right] = f_{\rm V}^2 \sum_{k=1}^{\infty} \frac{1}{s-(km_{\rm V})^2},$$

$$\mathcal{F}_{\rm A}(s) = \frac{f_{\rm A}^2}{m_{\rm A}^2}\left[\frac{\pi m_{\rm A}}{2\sqrt{s}}\cot\left(\frac{\pi\sqrt{s}}{m_{\rm A}}\right) - \frac{m_{\rm A}^2}{2s}\right] = f_{\rm A}^2 \sum_{k=1}^{\infty} \frac{1}{s-(km_{\rm A})^2}. \tag{7.20}$$

The vector meson poles are located at $km_{V,A}$, ($k=1,2,3,\ldots$), with decay constants $f_{V,A}$.

The expression for S in terms of the decay constants and masses is given by

$$S = 4\pi\zeta(2)\left[\frac{f_{\rm V}^2}{m_{\rm V}^2} - \frac{f_{\rm A}^2}{m_{\rm A}^2}\right], \quad \zeta(2) = \frac{\pi^2}{6}. \tag{7.21}$$

1. Dispersion relation: Cotangent model

The imaginary parts of $\mathcal{F}_{\rm V}(s)$ and $\mathcal{F}_{\rm A}(s)$ are

$$\mathrm{Im}\,\mathcal{F}_{\rm V}(s) = -\pi f_{\rm V}^2 \sum_{k=1}^{\infty} \delta(s-(km_{\rm V})^2),$$

$$\mathrm{Im}\,\mathcal{F}_{\rm A}(s) = -\pi f_{\rm A}^2 \sum_{k=1}^{\infty} \delta(s-(km_{\rm A})^2).$$

Using Eq. (3.2), we recover Eq. (7.21):

$$S = 4\pi\left[\frac{f_{\rm V}^2}{m_{\rm V}^2} - \frac{f_{\rm A}^2}{m_{\rm A}^2}\right]\sum_{k=1}^{\infty}\frac{1}{k^2} = 4\pi\zeta(2)\left[\frac{f_{\rm V}^2}{m_{\rm V}^2} - \frac{f_{\rm A}^2}{m_{\rm A}^2}\right].$$

Again, the Weinberg sum rules cannot be imposed. This time, instead of Eq. (7.18), we impose the condition

$$\frac{f_{\rm V}^2}{m_{\rm V}} - \frac{f_{\rm A}^2}{m_{\rm A}} = 0, \tag{7.22}$$

which has the effect of making the coefficient of the $1/\sqrt{s}$ term vanish in the limit $-s=Q^2\to\infty$. Again, we emphasize that our toy model is not motivated by any field theory and this condition is just to make it mimic QCD. Note that in contrast to all the previous models, imposing Eq. (7.22) will make $f_{\rm V}^2$ *smaller* than $f_{\rm A}^2$ since we naturally assume $m_{\rm V} < m_{\rm A}$. Therefore, we define

$$f_{\rm V}^2 - f_{\rm A}^2 = -2f_*^2.$$

Then,

$$f_{\rm V}^2 = \frac{2\sqrt{r}}{1-\sqrt{r}}f_*^2, \quad f_{\rm A}^2 = \frac{2}{1-\sqrt{r}}f_*^2, \quad r = \frac{m_{\rm V}^2}{m_{\rm A}^2},$$

and

$$S = 8\pi\zeta(2)\sqrt{r}\frac{f_*^2}{m_{\rm V}^2}.$$

If we identify f_*^2 with $f_{\rm TC}^2$, set $r=0.4$, and use the large-N relation Eq. (7.8), we find

$$S \approx 0.13 N_{\rm D} N_{\rm TC}.$$

2. ACD technique: Cotangent model

The large momentum expansion of our model function is trivial since the defining equation, Eq. (7.20), is already in the desired form. Imposing Eq. (7.22), we find

$$\mathcal{F}(s) = \frac{f_*^2}{s}\left[\frac{\pi\sqrt{s}}{(m_{\rm A}-m_{\rm V})}\left\{\cot\left(\frac{\pi\sqrt{s}}{m_{\rm V}}\right) - \cot\left(\frac{\pi\sqrt{s}}{m_{\rm A}}\right)\right\} + 1\right]. \tag{7.23}$$

Note that this relation is exact. It does not involve any approximation. Since

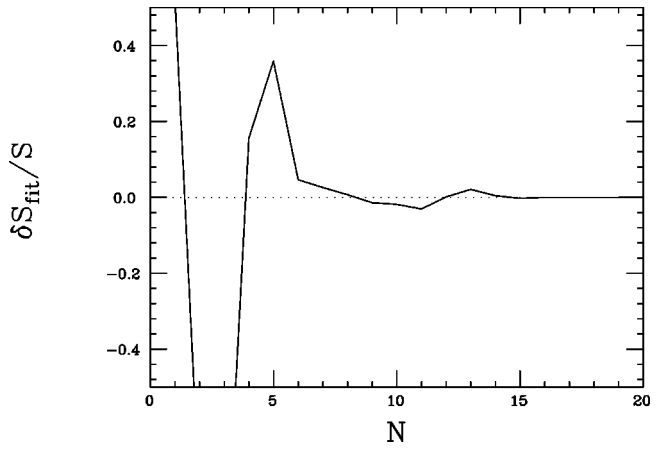

FIG. 18. The N dependence of the fit error for the Cotangent model.

$$\lim_{z\to i\infty}\cot(z)=-\lim_{-iz\to\infty}\coth(-iz)=-1,$$

Eq. (7.23) has a particularly simple form in the deep Euclidean region $-s=Q^2\gg 0$ where

$$\mathcal{F}(-Q^2)\sim-\frac{f_*^2}{Q^2}. \tag{7.24}$$

Therefore, the cotangent model is a rather unusual case in which the large momentum expansion has only one term. As a result, there is no truncation error.

The fit interval used was $s_0/m_{\rm V}^2=0.2$ and $R/m_{\rm V}^2=5$. This choice places 2 vector resonances and 1 axial-vector resonance within the fit interval. The fit routine was the least-squares fit. We used $r=m_{\rm V}^2/m_{\rm A}^2=0.4$. The results are shown in Figs. 18 and 19. Here, one does not encounter any surprises. The fit error converges while the analytic continuation error diverges. However, one must go up to $N=6$ for the fit error to be within 10%.

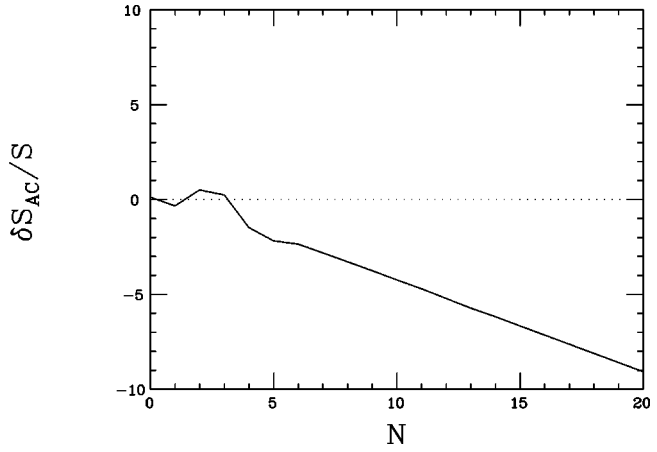

FIG. 19. The N dependence of the analytic continuation error for the Cotangent model.

VIII. SUMMARY AND CONCLUSIONS

In this paper, we have investigated in detail the validity of the analytic continuation by duality method in predicting the electroweak S parameter in technicolor models. We first identified the sources of error inherent in the ACD technique. They were:

(i) the fit error $\delta S_{\rm fit}(N)$,

(ii) the truncation error $\delta S_{\rm trunc}(N,M)$, and

(iii) the analytic continuation error $\delta S_{\rm AC}(N,M)$.

We then applied the ACD method to some toy models with spectral functions and large momentum expansions which mimic those of QCD and technicolor. In these toy models, the spectral functions, the coefficients of the large momentum expansion, and the actual value of S were all known exactly. Using this information, the dependence of the three errors on the order of the fit polynomial N and on the order of truncation of the large momentum expansion M was evaluated analytically for each model.

Based on these investigations, we conclude that the analytical continuation error is out of our control. This is not surprising given the rather crude approximation involved. The situation can be improved somewhat by including the s dependence of the large momentum expansion coefficients. However, even if this s dependence were known exactly, it does not guarantee the convergence of the truncation error. In applications to actual field theoretical models, the momentum dependence of the OPE coefficients can only be calculated perturbatively, giving rise to an additional source of error. In fact, the error coming from the uncertainty in the OPE coefficients may be completely uncontrollable given that the coefficients of the fit polynomial $a_n(N)$ diverge in the limit $N\to\infty$. A further complication results from the fact that the OPE is only an asymptotic series. Therefore going to higher orders may not improve the accuracy of the estimate. The fit error can be reduced by using a higher order fit polynomial. Yet we find that how fast it will converge depends greatly on the structure of the spectral function which is unknown.

We therefore conclude that the ACD technique cannot yield a reliable answer when used in the computation of S in theories such as walking technicolor where we neither have a good understanding of the particle spectrum nor do we know the OPE coefficients except approximately. Even for QCD-like technicolor theories, the fact that ACD reproduced the dispersion relation result should be considered a mere coincidence.

In retrospect, it is not surprising that the ACD method fails to yield a reliable estimate of S given that it is the $1/s$ moment of the spectral function while the OPE coefficients are all moments of order higher than 1. Mathematically, all different moments of any function are independent of one another and one cannot calculate one from a small subset of others.

ACKNOWLEDGMENTS

We would like to thank L. C. Goonetileke, W. Loinaz, M. E. Peskin, D. Sundrum, and K. Takeuchi for helpful discussions. T.T. would also like to thank the hospitality of the

Fermilab Theory Group where a portion of this work was carried out. This work was supported in part by the U.S. Department of Energy under Grant No. DEFG02-84ER40153 (S.R.I. and L.C.R.W.).

APPENDIX A: FITTING ROUTINES

In this appendix, we present the formulas for fitting a polynomial in s,

$$p_N(s)=\sum_{n=1}^{N} a_n s^n,$$

to $1/s$ in the interval $s\in[s_0,R]$. A simple change of variables,

$$x=-ps+q, \quad p=\frac{2}{R-s_0}, \quad q=\frac{R+s_0}{R-s_0},$$

converts the problem to that of fitting a polynomial in x,

$$\tilde{p}_N(x)=\sum_{k=1}^{N} b_k x^k,$$

to the function

$$f(x)=\frac{1}{x-q}, \quad q>1,$$

in the interval $x\in[-1,1]$. Once the x coefficients b_k's are obtained, the s coefficients a_n's can be determined from the relation

$$\sum_{n=0}^{N} a_n s^n=-p\sum_{k=0}^{N} b_k(-ps+q)^k.$$

Explicitly, the expression for a_n is given by

$$a_n=\sum_{k=n}^{N}\binom{k}{n}(-p)^{n+1}q^{k-n}b_k, \tag{A1}$$

where

$$\binom{k}{n}=\frac{k!}{n!(k-n)!}.$$

In *fitting* $\tilde{p}_N(x)$ to $f(x)$, the x coefficients b_k's are determined so that some *norm*[9] of the difference function

$$d(x)=f(x)-\tilde{p}_N(x)$$

on $[-1,1]$ is minimized.

[9]A *norm* of a function $f(x)$, which we will denote $\|f\|$, is a functional of $f(x)$ which satisfies the following properties: (1) $\|f\|\geqslant 0$ with equality if and only if $f(x)\equiv 0$. (2) $\|\lambda f\|=|\lambda|\|f\|$ for any scalar λ. (3) $\|f+g\|\leqslant\|f\|+\|g\|$.

It should be noted that the norm is not unique. Different fit routines correspond to different choices for the norm. In the following, we will look at several popular norms (i.e. fit routines) for determining the b_k's. They are all special cases of L_p norms which are defined by

$$\|d\|\equiv\left[\int_a^b |d(x)|^p w(x)dx\right]^{1/p},$$

where $w(x)$ is some weight function.

1. Least squares fit

Perhaps the most popular of all fit routines is the least squares fit which minimizes the L_2 norm:

$$\|d\|=\left[\int_a^b d(x)^2 w(x)dx\right]^{1/2}.$$

The popularity of this routine is due to the ease with which it can be applied.

The unweighted least squares fit $[w(x)=1]$ to a continuous function $f(x)$ in the interval $[-1,1]$ can be obtained by expanding $f(x)$ in Legendre polynomials:

$$P_n(x)=\frac{(-1)^n}{2^n n!}\frac{d^n}{dx^n}[(1-x^2)^n].$$

The explicit forms of the first few Legendre polynomials are given by

$$P_0(x)=1$$

$$P_1(x)=x$$

$$P_2(x)=\frac{1}{2}(3x^2-1)$$

$$P_3(x)=\frac{1}{2}(5x^2-1)$$

$$P_4(x)=\frac{1}{8}(35x^4-30x^2+3)$$

$$\vdots$$

and the subsequent ones can be obtained using the recursion relation

$$P_n(x)=\frac{2n-1}{n}xP_{n-1}(x)-\frac{n-1}{n}P_{n-2}(x). \tag{A2}$$

Since the Legendre polynomials are orthonormal on $[-1,1]$,

$$\int_{-1}^{1} P_n(x)P_m(x)dx=\frac{2}{2n+1}\delta_{mn},$$

we can expand any ''well-behaved'' function into a Fourier-Legendre series:

$$f(x)=\sum_{n=0}^{\infty}\frac{2n+1}{2}c_nP_n(x),$$

where

$$c_n=\int_{-1}^{1}f(\xi)P_n(\xi)d\xi. \tag{A3}$$

The series is truncated after $N+1$ terms and the obtained polynomial is our approximation to $f(x)$:

$$\sum_{n=0}^{N}\frac{2n+1}{2}c_nP_n(x)=\tilde{p}_N(x)=\sum_{k=0}^{N}b_kx^k.$$

Therefore, the problem is reduced to finding the c_n's and converting the Fourier-Legendre series into a power series.

The expansion coefficients, Eq. (A3), for the function

$$f(x)=\frac{1}{x-q},\quad q>1,$$

can be found by the so-called Neumann's formula [24]

$$Q_n(q)=\frac{1}{2}\int_{-1}^{1}\frac{P_n(t)}{q-t}dt=-\frac{c_n}{2},$$

where

$$Q_n(q)=\frac{1}{2}P_n(q)\ln\frac{q+1}{q-1}-\sum_{j=0}^{\left[\frac{n-1}{2}\right]}\frac{2n-4j-1}{(2j+1)(n-j)}P_{n-2j-1}(q)$$

is the Legendre function of the second kind. By convention, $P_{-1}(q)=0$. Therefore,

$$\tilde{p}_N(x)=-\sum_{n=0}^{N}(2n+1)Q_n(q)P_n(x).$$

The explicit forms for the first few $Q_n(q)$'s can be found, for instance, in Ref. [25]. However, the easiest way to calculate the $Q_n(q)$'s is to use the following recursion relations:

$$Q_0(q)=\frac{1}{2}\ln\frac{q+1}{q-1}=\frac{1}{2}\ln\frac{R}{s_0},$$

$$Q_1(q)=qQ_0(q)-1,$$

$$Q_n(q)=\frac{2n-1}{n}qQ_{n-1}(q)-\frac{n-1}{n}Q_{n-2}(q),\quad n\geqslant 2.$$

For the more general weighted case, the integral

$$I=\|d\|^2=\int_{s_0}^{R}\left(\frac{1}{s}-\sum_{n=0}^{N}a_ns^n\right)^2w(s)ds$$

is minimized by choosing the coefficients a_n so that they satisfy the conditions

$$\frac{\delta I}{\delta a_i}=0,\quad i=0,1,\ldots,N.$$

This leads to the system of linear equations

$$\sum_{j=0}^{N}M_{ij}a_j=v_i,\quad i=0,1,\ldots,N,$$

where

$$M_{ij}=\int_{s_0}^{R}s^{i+j}w(s)ds,\quad v_i=\int_{s_0}^{R}s^{i-1}w(s)ds.$$

Therefore, the problem is reduced to that of inverting the matrix $M=(M_{ij})$.

2. Minimax fit

The minimax approximation, also called the best uniform approximation, *min*imizes the *max*imal distance $\max|d(x)|$ between the polynomial $\tilde{p}_N(x)$ and the function $f(x)$ on the interval $[a,b]$. That is, it minimizes the norm

$$\|d\|=\max_{x\in[a,b]}|d(x)|.$$

(This corresponds to the L_∞ norm though it is not obvious at first sight. See Ref. [28].)

The minimax fit to the function

$$f(x)=\frac{1}{x-q},\quad q>1,$$

on the interval $[-1,1]$ is given by ([23], exercise 1.20, p. 45)

$$\tilde{p}_N(x)=\sum_{k=0}^{N}b_kx^k=\frac{-2t}{t^2-1}+\frac{4t}{t^2-1}\sum_{n=0}^{N-1}t^nT_n(x)-\frac{4t^{N+1}}{(t^2-1)^2}T_N(x),$$

where

$$T_n(\cos\theta)\equiv\cos n\theta$$

are the Chebyshev polynomials[10] and

[10]An alternative definition of Chebyshev polynomials is given by

$$T_n(x)\equiv\frac{(-1)^n}{(2n-1)!!}\sqrt{1-x^2}\frac{d^n}{dx^n}[(1-x^2)^{n-1/2}].$$

$$t = q - \sqrt{q^2 - 1}.$$

The x coefficients b_k's are most easily obtained using the explicit forms for the Chebyshev polynomials:

$$T_0(x) = 1$$

$$T_1(x) = x$$

$$T_2(x) = 2x^2 - 1$$

$$T_3(x) = 4x^3 - 3x$$

$$T_4(x) = 8x^4 - 8x^2 + 1$$

$$\vdots$$

Subsequent Chebyshev polynomials can be obtained from the recursion relation

$$T_{n+1}(x) = 2xT_n(x) - T_{n-1}(x). \tag{A4}$$

According to the Chebyshev theorem [23], [theorem 1.7, p. 26] the difference function $d(x)$ reaches its extreme values at $N+2$ points: at the ends of the interval (at s_0 and R) and at N points in between. Once we have found the polynomial $p_N(s)$ we can easily find the maximal distance

$$d_{\max} = |d(s_0)| = \frac{1}{s_0} - p_N(s_0).$$

This distance may be used to find an upper bound of an integral containing $d(s)$, e.g.

$$\left| \int d(s)g(s)ds \right| \leqslant \int |d(s)||g(s)|ds < d_{\max} \int |g(s)|ds.$$

3. Least-first-power fit

The least-first-power fit minimizes the L_1 norm:

$$\|d\| = \int_a^b |d(x)| w(x) dx.$$

The unweighted least-first-power fit $[w(x) \equiv 1]$ is of particular interest as it minimizes the area enclosed by the graphs $f(x)$ and $p_N(x)$ for $x \in [a,b]$. We have concentrated on this ''minimal area'' fit.

The minimal area fit for a function $f(x)$ can be obtained with relative ease if the function $f(x)$ is such that the difference $d(x) = f(x) - \tilde{p}_N(x)$ has at most $N+1$ distinct zeros in $[-1,1]$ for any $\tilde{p}_N(x)$. In this case, the polynomial $\tilde{p}_N(x)$ which minimizes the unweighted L_1 norm in the interval $[-1,1]$ can be shown to satisfy ([23], corollary 3.4.1, p. 73)

$$\tilde{p}_N(x_j) = f(x_j), \quad j = 1, \ldots, N+1, \tag{A5}$$

where

$$x_j \equiv \cos \frac{j\pi}{N+2}.$$

For the function

$$f(x) = \frac{1}{x - q},$$

the polynomial which satisfies this condition is given by

$$\tilde{p}_N(x) = \sum_{n=0}^{N} c_n U_n(x),$$

where

$$U_n(\cos\theta) \equiv \frac{\sin(n+1)\theta}{\sin\theta}$$

are the Chebychev polynomials of the second kind[11] and

$$c_n = -2\frac{U_{N-n}(q)}{U_{N+1}(q)}.$$

Explicitly, the $U_n(x)$'s are given by

$$U_0(x) = 1$$

$$U_1(x) = 2x$$

$$U_2(x) = 4x^2 - 1$$

$$U_3(x) = 8x^3 - 4x$$

$$U_4(x) = 16x^4 - 12x^2 + 1$$

$$\vdots$$

and subsequent ones can be obtained from the recursion relation

$$U_n(x) = 2xU_{n-1}(x) - U_{n-2}(x),$$

which is the same as Eq. (A4).

To show that $\tilde{p}_N(x)$, with the c_n's given above, does indeed satisfy the condition

$$\sum_{n=0}^{N} c_n U_n(x_j) = \frac{1}{x_j - q}, \quad j = 1, \ldots, N+1, \tag{A6}$$

we start with the relationship

$$U_{N-n}(q) = U_{N+1}(q)T_{n+1}(q) - U_n(q)T_{N+2}(q),$$

which follows trivially from trigonometric identities. From this, we find

[11] An alternative definition is

$$U_n(x) \equiv \frac{(-1)^n(n+1)}{(2n+1)!!} \frac{1}{\sqrt{1-x^2}} \frac{d^n}{dx^n}[(1-x^2)^{n+1/2}].$$

$$2\sum_{n=0}^{N} U_{N-n}(q)U_n(x) = 2U_{N+1}(q)\sum_{n=0}^{N} T_{n+1}(q)U_n(x) - 2T_{N+2}(q)\sum_{n=0}^{N} U_n(q)U_n(x). \tag{A7}$$

The sums on the right-hand side of Eq. (A7) are obtained from specializations of the Christoffel-Darboux formula to Chebyshev polynomials in literature on special functions (e.g. in [27]). After some rearrangements on the right-hand side,

$$2\sum_{n=0}^{N} U_{N-n}(q)U_n(x) = \frac{U_{N+1}(x)-U_{N+1}(q)}{x-q}. \tag{A8}$$

Since

$$U_{N+1}(x_j)=0, \quad j=1,\ldots,N+1,$$

the formula (A8) yields

$$-\frac{2}{U_{N+1}(q)}\sum_{n=0}^{N} U_{N-n}(q)U_n(x_j)=\frac{1}{x_j-q},$$

$$j=1,\ldots,N+1,$$

which proves Eq. (A6) with the c_n's given above.

4. Comparison of the fit routines

The Legendre polynomials, used in the unweighted least squares fit, are orthonormal on $[-1,1]$ *with the weight 1*. On the other hand, the orthonormality relations for the Chebyshev polynomials are

(i) first kind (minimax fit)

$$\int_{-1}^{1}\frac{1}{\sqrt{1-x^2}}T_m(x)T_n(x)dx=\frac{\pi}{2}(\delta_{mn}+\delta_{m0}\delta_{n0}),$$

(ii) second kind (least-first-power fit)

$$\int_{-1}^{1}\sqrt{1-x^2}U_m(x)U_n(x)dx=\frac{\pi}{2}\delta_{mn}.$$

If we use the relations

$$T_n(\cos\theta)=\cos n\theta, \quad U_n(\cos\theta)=\frac{\sin(n+1)\theta}{\sin\theta},$$

we note that the above orthonormality relations are simply those of trigonometric functions.

Clearly, if we take the unweighted least squares fit as ''unbiased,'' the minimax fit is ''weighted'' towards the ends of the interval while the (unweighted) least-first-power fit tends to be better in the middle of the interval.

APPENDIX B: FORMULAS FOR CALCULATING THE EXPANSION COEFFICIENTS FOR THE PERTURBATIVE SPECTRAL FUNCTION

In this appendix, we present the formulas for calculating the expansion coefficients for the perturbative spectral function.

Let us write the perturbative model function as

$$\mathcal{F}_{\rm pert}(s)=-\frac{x}{4\pi^2}\left(2-\beta\ln\frac{\beta+1}{\beta-1}\right)=-\frac{x}{4\pi^2}\left[2+\sqrt{1-4x}\ln(-x)-2\sqrt{1-4x}\ln\frac{\sqrt{1-4x}+1}{2}\right],$$

where

$$x\equiv\frac{m^2}{s}, \quad \beta=\sqrt{1-4x}.$$

The factor $\sqrt{1-4x}$ can be expanded into a Taylor-McLaurin series for small x (i.e. for large s) using the Newton binomial formula

$$\sqrt{1-4x}=\sum_{n=0}^{\infty}\binom{\frac{1}{2}}{n}(-4)^n x^n\equiv\sum_{n=0}^{\infty} g_n x^n$$

where

$$\binom{\frac{1}{2}}{0}=1,$$

$$\binom{\frac{1}{2}}{n}=\frac{\frac{1}{2}\left(\frac{1}{2}-1\right)\cdots\left(\frac{1}{2}-n+1\right)}{n!}=\frac{(-1)^{n-1}(2n-3)!!}{2^n n!} \quad (n\geqslant 1).$$

[We use the convention $(-1)!!=1$.] Therefore, we find the following recursion relation for g_n:

$$g_0=1, \quad g_n=\frac{2(2n-3)}{n}g_{n-1} \quad (n\geqslant 1).$$

Similarly,

$$f(x)\equiv\frac{\sqrt{1-4x}+1}{2}=1+\sum_{n=1}^{\infty}\frac{g_n}{2}x^n\equiv 1+\sum_{n=1}^{\infty} f_n x^n$$

so that the function $\ln\{f(x)\}$ can be expanded into a Taylor-McLaurin series using the formula [26]

$$\ln\{f(x)\}=\sum_{m=1}^{\infty} l_m x^m,$$

where

$$m l_m = m f_m - \sum_{k=1}^{m-1} (m-k) f_k l_{m-k}.$$

Therefore,

$$\sqrt{1-4x}\ln\frac{\sqrt{1-4x}+1}{2}=\left[\sum_{n=0}^{\infty} g_n x^n\right]\left[\sum_{m=1}^{\infty} l_m x^m\right]\equiv\sum_{i=0}^{\infty} h_i x^i,$$

where

$$h_i=\sum_{j=0}^{i-1} g_j l_{i-j}.$$

We can of course use symbolic calculation programs such as MATHEMATICA or MAPLE V to obtain the expansion coefficients explicitly. The first 10 terms of the expansion are given by

$$\begin{aligned}-4\pi^2\mathcal{F}_{\rm pert}(s)=&x\left\{-\ln\left(-\frac{1}{x}\right)+2\right\}+x^2\left\{2\ln\left(-\frac{1}{x}\right)+2\right\}\\&+x^3\left\{2\ln\left(-\frac{1}{x}\right)-1\right\}+x^4\left\{4\ln\left(-\frac{1}{x}\right)-\frac{10}{3}\right\}+x^5\left\{10\ln\left(-\frac{1}{x}\right)-\frac{59}{6}\right\}\\&+x^6\left\{28\ln\left(-\frac{1}{x}\right)-\frac{449}{15}\right\}+x^7\left\{84\ln\left(-\frac{1}{x}\right)-\frac{1417}{15}\right\}+x^8\left\{264\ln\left(-\frac{1}{x}\right)-\frac{32254}{105}\right\}\\&+x^9\left\{858\ln\left(-\frac{1}{x}\right)-\frac{429697}{420}\right\}+x^{10}\left\{2860\ln\left(-\frac{1}{x}\right)-\frac{437705}{126}\right\}+\cdots.\end{aligned}$$

APPENDIX C: FORMULAS FOR CALCULATING THE ERRORS FOR THE PERTURBATIVE SPECTRAL FUNCTION

The fit error for the perturbative spectral function

$$\mathrm{Im}\,\mathcal{F}_{\rm pert}(s)=-\frac{1}{4\pi}\frac{m^2}{s}\beta\theta(s-4m^2),\quad \beta=\sqrt{1-\frac{4m^2}{s}},$$

can be calculated analytically as follows:

$$\begin{aligned}\delta S_{\rm fit}&=\frac{m^2}{\pi}\int_{4m^2}^{R} ds\left[\frac{1}{s}-\sum_{n=0}^{N} a_n(N)s^n\right]\frac{\beta}{s}\\&=\frac{1}{2\pi}\int_0^{\beta_R} d\beta\,\beta^2\left[1-\sum_{n=0}^{N} a_n(N)s^{n+1}\right]\\&=\frac{1}{2\pi}\left[\frac{\beta_R^3}{3}-\sum_{n=0}^{N} a_n(N)I_n\right],\end{aligned}$$

where

$$\beta_R\equiv\sqrt{1-\frac{4m^2}{R}},$$

and the integrals

$$\begin{aligned}I_n&\equiv\int_0^{\beta_R} d\beta\,\beta^2 s^{n+1}=(4m^2)^{n+1}\int_0^{\beta_R} d\beta\frac{\beta^2}{(1-\beta^2)^{n+1}}\\&\equiv(4m^2)^{n+1}J_n\end{aligned}$$

can be calculated using the recursion relation

$$J_0=\frac{1}{2}\ln\left(\frac{1+\beta_R}{1-\beta_R}\right)-\beta_R$$

$$J_n=\left(\frac{2n-3}{2n}\right)J_{n-1}+\frac{1}{2n}\frac{\beta_R^3}{(1-\beta_R^2)^n}\quad(n\geqslant 1).$$

The analytic continuation error is calculated as follows: Note that the coefficients of the large momentum expansion can be written as

$$\begin{aligned}h_i(s)&=f_i\ln\frac{-s}{m^2}+g_i=f_i\ln\frac{-s}{R}+\left(f_i\ln\frac{R}{m^2}+g_i\right)\\&=f_i\ln\frac{-s}{R}+\hat{h}_i.\end{aligned}$$

Therefore,

$$\begin{aligned}\delta S_{\rm AC}&=-\frac{2}{i}\oint_{|s|=R} ds\left[\frac{1}{s}-\sum_{i=0}^{N} a_i(N)s^i\right]\sum_{j=1}^{M}\frac{f_j}{s^j}\ln\frac{-s}{R}\\&=-4\pi\left[\sum_{j=1}^{M} f_j\left(\frac{1}{2\pi i}\oint_{|s|=R} ds\,s^{-j-1}\ln\frac{-s}{R}\right)\right.\\&\quad\left.-\sum_{i=0}^{N}\sum_{j=1}^{M} a_i(N)f_j\left(\frac{1}{2\pi i}\oint_{|s|=R} ds\,s^{i-j}\ln\frac{-s}{R}\right)\right].\end{aligned}$$

The integrals in the above expression are straightforward:

$$\oint_{|s|=R} ds\,s^k\ln\frac{-s}{R}=2\pi i\frac{R^{k+1}}{k+1}\quad(k\neq -1)$$

$$\oint_{|s|=R}\frac{ds}{s}\ln\frac{-s}{R}=0.$$

Since the calculation of S_{ACD} is trivial, and the exact value of S is known, the truncation error can be obtained from

$$\delta S_{\mathrm{trunc}} = S - S_{\mathrm{ACD}} - \delta S_{\mathrm{AC}} - \delta S_{\mathrm{fit}}.$$

APPENDIX D: FORMULAS FOR CALCULATING THE FIT ERROR FOR THE BREIT-WIGNER MODEL

The fit error for the Breit-Wigner model,

$$\mathrm{Im}\,\mathcal{F}(s) = -f_{\mathrm{V}}^2 \frac{\sqrt{s}\Gamma_{\mathrm{V}}}{(s-m_{\mathrm{V}}^2)^2 + s\Gamma_{\mathrm{V}}^2} + f_{\mathrm{A}}^2 \frac{\sqrt{s}\Gamma_{\mathrm{A}}}{(s-m_{\mathrm{A}}^2)^2 + s\Gamma_{\mathrm{A}}^2}, \tag{D1}$$

can be found analytically. From the expression for the fit error,

$$\delta S_{\mathrm{fit}} = -4\int_{s_0}^{R} ds \left[\frac{1}{s} - \sum_{n=0}^{N} a_n(N) s^n\right] \mathrm{Im}\,\mathcal{F}(s), \tag{D2}$$

and Eq. (D1) we conclude that all the involved integrals have the form of the following indefinite integral:

$$\int ds \frac{s^{n-1}\sqrt{s}}{(s-m^2)^2 + s\Gamma^2} = 2\int dq \frac{q^{2n}}{q^4 + bq^2 + c} \equiv 2I_n,$$

where

$$b \equiv \Gamma^2 - 2m^2, \quad c \equiv m^4 \quad (b^2 - 4c < 0).$$

It is straightforward to derive the following recursion relation for the integral I_n:

$$I_{n+2} = \frac{q^{2n+1}}{2n+1} - bI_{n+1} - cI_n, \tag{D3}$$

with I_0 and I_1 found from tables (e.g. [29]):

$$I_0 = \frac{1}{4k^3} f_+(q,k,\alpha),$$

$$I_1 = \frac{1}{4k} f_-(q,k,\alpha),$$

where[12]

$$f_\pm(q,k,\alpha) = \frac{1}{2\cos(\alpha/2)} \ln \frac{q^2 \pm 2kq\cos(\alpha/2) + k^2}{q^2 \mp 2kq\cos(\alpha/2) + k^2} + \frac{1}{\sin(\alpha/2)} \arctan \frac{2kq\sin(\alpha/2)}{k^2 - q^2}$$

and

$$\cos\alpha \equiv -\frac{b}{2\sqrt{c}}, \quad k \equiv c^{1/4} = m.$$

Although Eq. (D3) is convenient for calculations, we proceed to derive an explicit expression for I_n since, for large n, this provides better numerical accuracy. The recursion relation, Eq. (D3), is equivalent to the following second-order linear difference equation:

$$\Delta^2 I_n + (b+2)\Delta I_n + (b+c+1) I_n = \frac{q^{2n+1}}{2n+1}, \tag{D4}$$

where

$$\Delta I_n \equiv I_{n+1} - I_n.$$

Equation (D4) with ''boundary conditions'' at I_0 and I_1 (which are, in turn, given by the explicit expressions above) is analogous to a boundary value problem for the corresponding differential equation. The general solution of the homogeneous equation corresponding to Eq. (D4) is

$$\overline{J_n} = \rho^n (A\cos n\alpha + B\sin n\alpha),$$

where $\rho = \sqrt{c} = m^2$ and α are the modulus and the absolute value of the argument, respectively, of the solutions of the auxiliary equation for Eq. (D4). The (discontinuous) Green's function for the problem is constructed by taking $G(n;j) = 0$ for $n > j$ and matching this solution to the general solution at $n = j+1$ [30]; the result is

$$G(n;j) = \frac{\rho^{n-j}}{\rho^2 \sin\alpha} \sin(n-j-1)\alpha \quad (n \leqslant j).$$

The solution of Eq. (D4) which satisfies the boundary conditions consists of a particular solution which accounts for the inhomogeneity ($I_0 \neq 0; I_1 \neq 1$) of the boundary conditions and of a sum involving the Green's function (analogous to the integral that would appear in the continuous case):

[12]For $q > k$ we must add π to the (negative) principal value of the arctan function. This can be seen from the fact that the integrand of $I_0 + I_1$ is positively definite and thus $I_0 + I_1 > 0$ which means that the arctan must be positive as well.

$$I_n=\frac{\rho^{n-1}}{\sin\alpha}\Bigg[I_1\sin n\alpha-\rho I_0\sin(n-1)\alpha + \sum_{j=0}^{n-2}\frac{\rho^{-j-1}q^{2j+1}}{2j+1}\sin(n-j-1)\alpha\Bigg] \quad (n\geqslant 2). \tag{D5}$$

With a bit of clairvoyance, this result can be derived from the formula [31]

$$\sum_{j=1}^{n} r^j\sin j\alpha=\frac{r\sin\alpha-r^{n+1}\sin(n+1)\alpha+r^{n+2}\sin n\alpha}{1-2r\cos\alpha+r^2}$$

by switching $n\to n-1$, taking $r=\rho/q^2$ and then integrating over q.

[1] S. L. Glashow, Nucl. Phys. **22**, 579 (1961); S. Weinberg, Phys. Rev. Lett. **19**, 1264 (1967); A. Salam, in *Elementary Particle Theory: Relativistic Groups and Analyticity (Nobel Symposium No. 8)*, edited by N. Svartholm (Almqvist and Wiksell, Stockholm, 1968).

[2] J. L. Hewett, T. Takeuchi, and S. Thomas, in *Electroweak Symmetry Breaking and New Physics at the TeV Scale*, edited by T. L. Barklow *et al.* (World Scientific, Singapore, 1997), Chap. 10, hep-ph/9603391; A. K. Grant and T. Takeuchi, hep-ph/9807413; T. Takeuchi, A. K. Grant, and W. Loinaz, in the *Proceedings of Hadron 13*, edited by B. S. Acharya *et al.* (World Scientific, Singapore, 1999), hep-ph/9904207.

[3] M. E. Peskin and T. Takeuchi, Phys. Rev. Lett. **65**, 964 (1990); Phys. Rev. D **46**, 381 (1992); T. Takeuchi, in *Proceedings of the International Workshop on Electroweak Symmetry Breaking*, edited by W. A. Bardeen, J. Kodaira, and T. Muta (World Scientific, Singapore, 1992).

[4] P. Sikivie, L. Susskind, M. Voloshin, and V. Zakharov, Nucl. Phys. **B173**, 189 (1989).

[5] D. C. Kennedy and B. W. Lynn, Nucl. Phys. **B322**, 1 (1989).

[6] R. Renken and M. E. Peskin, Nucl. Phys. **B211**, 93 (1983); B. W. Lynn, M. E. Peskin, and R. G. Stuart, in ''Physics at LEP,'' CERN Report No. CERN-89-08, edited by J. Ellis and R. Peccei, Vol. 1; M. Golden and L. Randall, Nucl. Phys. **B361**, 3 (1991); B. Holdom and J. Terning, Phys. Lett. B **247**, 88 (1990); R. Johnson, B.-L. Young, and D. W. McKay, Phys. Rev. D **43**, R17 (1991); A. Dobado, D. Espriu, and M. J. Herrero, Phys. Lett. B **255**, 405 (1991).

[7] J. Gasser and H. Leutwyler, Ann. Phys. (N.Y.) **18**, 142 (1984); Nucl. Phys. **B250**, 465 (1985).

[8] T. Appelquist, M. B. Einhorn, T. Takeuchi, and L. C. R. Wijewardhana, Phys. Lett. B **232**, 211 (1989).

[9] R. Jackiw and K. Johnson, Phys. Rev. D **8**, 2386 (1973).

[10] H. Pagels and S. Stokar, Phys. Rev. D **20**, 2947 (1979); T. Appelquist, M. B. Einhorn, T. Takeuchi, and L. C. R. Wijewardhana, *ibid.* **41**, 3192 (1990); V. A. Miransky, M. Tanabashi, and K. Yamawaki, Mod. Phys. Lett. A **4**, 1043 (1989); Phys. Lett. B **221**, 177 (1989); B. Holdom, *ibid.* **226**, 137 (1989).

[11] G. 't Hooft, Nucl. Phys. **B72**, 461 (1974); S. Coleman, *Aspects of Symmetry* (Cambridge University Press, Cambridge, England, 1985), Chap. 8. For a good collection of reprints concerning large-N approximations in general, see *The Large-N Expansion in Quantum Field Theory and Statistical Physics, from spin systems to 2-dimensional gravity*, edited by E. Brézin and S. R. Wadia (World Scientific, Singapore, 1993).

[12] N. F. Nasrallah, N. A. Papadopoulos, and K. Schilcher, Phys. Lett. **113B**, 61 (1982); **126B**, 379 (1983); **134B**, 355 (1984); Z. Phys. C **16**, 323 (1983); K. Schilcher and M. D. Tran, Phys. Rev. D **29**, 570 (1984); M. Kremer, N. A. Papadopoulos, and K. Schilcher, Phys. Lett. **143B**, 476 (1984); N. A. Papadopoulos, J. A. Peñarocha, F. Scheck, and K. Schilcher, *ibid.* **149B**, 213 (1984); Nucl. Phys. **B258**, 1 (1985); C. A. Dominguez, M. Kremer, N. A. Papadopoulos, and K. Schilcher, Z. Phys. C **27**, 481 (1985); M. Kremer, N. F. Nasrallah, N. A. Papadopoulos, and K. Schilcher, Phys. Rev. D **34**, 2127 (1986); N. A. Papadopoulos and H. Vogel, Phys. Lett. B **199**, 113 (1987); Phys. Rev. D **40**, 3722 (1989); Z. Phys. C **51**, 73 (1991); J. Liu and D. Liu, Chin. Phys. Lett. **9**, 225 (1992).

[13] R. Sundrum and S. D. H. Hsu, Nucl. Phys. **B391**, 127 (1993). The ACD technique has also been used in the technicolor context to calculate corrections to the $Zb\bar{b}$ vertex in U. Mahanta, Phys. Rev. D **51**, 3557 (1995).

[14] M. A. Shifman, A. I. Vainshtein, and V. I. Zakharov, Nucl. Phys. **B147**, 385 (1979); V. A. Novikov, M. A. Shifman, A. I. Vainshtein, and V. I. Zakharov, Fortschr. Phys. **32**, 585 (1984); Nucl. Phys. **B249**, 445 (1985); E. Bagan, M. R. Ahmady, V. Elias, and T. G. Steele, Z. Phys. C **61**, 157 (1994). For a good collection of reprints with up to date commentary concerning the application of the OPE to QCD, see *Vacuum Structure and QCD Sum Rules*, Current Physics—Sources and Comments, edited by M. A. Shifman (North-Holland, Amsterdam, 1992), Vol. 10.

[15] B. Holdom, Phys. Lett. **150B**, 301 (1985); T. Appelquist, D. Karabali, and L. C. R. Wijewardhana, Phys. Rev. Lett. **57**, 957 (1986); K. Yamawaki, M. Bando, and K. Matsumoto, *ibid.* **56**, 1335 (1986); T. Appelquist and L. C. R. Wijewardhana, Phys. Rev. D **36**, 568 (1987).

[16] M. Harada and Y. Yoshida, Phys. Rev. D **50**, 6902 (1994).

[17] I. Caprini and C. Verzegnassi, Nuovo Cimento A **80**, 187 (1984); P. Prešnajder and T. D. Spearman, Czech. J. Phys., Sect. B **37**, 1089 (1987); S. Narison, *QCD Spectral Sum Rules* (World Scientific, Singapore, 1989).

[18] S. R. Ignjatović, T. Takeuchi, and L. C. R. Wijewardhana, Phys. Lett. B **401**, 287 (1997); T. Takeuchi, L. C. Goonetileke, S. R. Ignjatović, and L. C. R. Wijewardhana, in *the Proceedings of SCGT'96*, edited by J. Nishimura and K. Yamawaki (World Scientific, Singapore, 1997), hep-ph/9702439; S. R. Ignjatović, Ph.D. thesis, University of Cincinnati, 1997.

[19] R. Shankar, Phys. Rev. D **15**, 755 (1977).

[20] S. Weinberg, Phys. Rev. Lett. **18**, 507 (1967).
[21] G. J. Gounaris and J. J. Sakurai, Phys. Rev. Lett. **21**, 244 (1968).
[22] M. A. Shifman, in Proceedings of Minneapolis '94, Continuous Advances in QCD, edited by A. V. Smilga (World Scientific, River Edge, NJ, 1994), hep-ph/9405246; in Proceedings of PASCOS/Hopkins '95, edited by J. Bagger *et al.* (World Scientific, Singapore, 1996), hep-ph/9505289.
[23] T. J. Rivlin, *An Introduction to the Approximation of Functions* (Blaisdell, Waltham, MA, 1969).
[24] W. W. Bell, *Special Functions for Scientists and Engineers* (D. Van Nostrand, London, 1968).
[25] *Handbook of Mathematical Functions*, edited by M. Abramowitz and I. Stegun (Dover, New York, 1965).
[26] F. W. J. Olver, *Asymptotics and Special Functions* (Academic Press, New York, 1974).
[27] W. Magnus, F. Oberhettinger and R. P. Soni, *Formulas and Theorems for the Special Functions of Mathematical Physics* (Springer-Verlag, New York, 1966).
[28] The result known as the *Polya algorithm* states that the sequence of best $L_1, L_2, \ldots, L_p$ approximations to a continuous function converges to the minimax approximation as $p \to \infty$ (if the minimax approximation exists). See J. P. Rice, *The Approximation of Functions* (Addison-Wesley, Reading, MA, 1964), Vol. I.
[29] G. Petit Bois, *Tables of Indefinite Integrals* (Dover, New York, 1961).
[30] P. M. Morse and H. Feshbach, *Methods of Theoretical Physics* (McGraw-Hill, New York, 1953), Vol. I, pp. 701–705.
[31] The formula is derived starting from $e^{in\alpha} = \cos n\alpha + i \sin n\alpha$; it is given on p. 307 of Staff of Research and Education Association, *Handbook of Mathematical, Scientific, and Engineering Formulas, Tables, Functions, Graphs, Transforms* (REA, New York, 1984).